THE ASTROPHYSICAL JOURNAL, 426:170–191, 1994 May 1

CHEMICAL EVOLUTION OF THE ORION ASSOCIATION. II. THE CARBON, NITROGEN, OXYGEN, SILICON, AND IRON ABUNDANCES OF MAIN-SEQUENCE B STARS

KATIA CUNHA[1,2] AND DAVID L. LAMBERT[2]
Received 1993 September 17; accepted 1993 November 3

ABSTRACT

Carbon, nitrogen, oxygen, and silicon abundances are presented from LTE and non-LTE analyses of C II, N II, and Si III lines in the spectra of 18 main-sequence B stars from the four subgroups comprising the Orion association. Iron LTE abundances from Fe III lines are also presented. The C, N, and Fe abundances show no significant variations across the subgroups, but the O and Si abundances are found to be higher for some of the youngest stars that are collocated on the sky and at a common distance. The O and Si abundances are correlated. Although such a correlation may in part reflect measurement errors, it is suggested that the enrichment of young stars in O and Si arose because they were formed from regions of the molecular cloud enriched with the ejecta of Type II supernovae, which are predicted to be rich in O and Si but not in C and N. With the exception of one star, we see no evidence for CN-cycled material on the stars' surfaces. The stellar abundances agree, within the expected uncertainties, with published nebular analyses that show Orion to be slightly underabundant in C, N, and O relative to the Sun.

Subject headings: open clusters and associations: individual (Orion I) — stars: abundances — stars: early-type

1. INTRODUCTION

A fascinating window into certain aspects of stellar evolution and nucleosynthesis is provided by the chemical composition of the stars in an OB association. The physical processes taking place in such associations can also provide important clues to the understanding of other astrophysical problems such as star formation, the origin of the cosmic rays, and even the origin of the solar system. Probably all O and B stars form in OB associations, and on a galactic timescale the birth, evolution, and death of these massive stars occur almost simultaneously. OB assocations have lifetimes of $(1–2) \times 10^7$ yr (Reeves 1978) and may consist of distinct stellar generations. Lifetimes of massive O stars can be as short as few million years; such stars end their evolution as Type II supernovae and may pollute the interstellar gas in their OB association. Since star formation occurs over the lifetime of the OB association, later generations of stars may have formed out of material whose chemical composition has been altered by supernovae within the association. This idea of self-enrichment was examined first by Reeves (1972, 1978) and later by Olive & Schramm (1982). In this series of papers, we examine the chemical composition of stars in the Orion association for evidence of self-enrichment.

The Orion association is the most extensively studied OB association. It is situated at a distance of about 500 pc from the Sun and 130 pc away from the Galactic plane. It consists of four subgroups, Ia, Ib, Ic, and Id, of different locations, sizes, and ages, suggesting that star formation in this region has spread progressively through the molecular cloud. The time lag of about 11 Myr (see review by Blaauw 1991) between the formation of the oldest (subgroup Ia) and the youngest (subgroup Id) subgroups is comparable to the lifetime of massive stars, so that the most massive stars would have had time to explode as supernovae (Reeves 1978), possibly changing the composition of the gas during the lifetime of the association. There is certainly observational evidence that supernova (SN) explosions have occurred in the Orion association (Goudis 1982 and references therein): (1) The expanding shells comprising Barnard's Loop and the associated filamentary structure surrounding the association. (2) High-velocity shells detected from observations of ultraviolet absorption lines; these shells are believed to represent radiative shocks of one or more supernova remnants. (3) The existence of runaway stars such as AE Aur, μ Col, and 53 Ari, which are moving away from the Orion association with high velocities, and probably had their origin in explosive events in close binary systems in the Orion association.

The Orion association seemed therefore well suited to the search for self-enrichment caused by supernova explosions. In the first paper of this series, we derived the oxygen abundances of 18 main-sequence B stars in Orion, belonging to the four subgroups (Cunha & Lambert 1992, hereafter Paper I), and we presented evidence for a modest degree of self-enrichment within the Orion association. In the present paper we continue that study, and we present LTE and NLTE abundances of carbon, nitrogen and silicon, and LTE abundances of iron and re-discuss the oxygen abundances for the same 18 main sequence stars. Section 2 discusses the observations. In § 3 we discuss the effective temperatures and surface gravities of the stars and we derive LTE and non-LTE (NLTE) abundances. In § 4 we discuss the implications for self-enrichment in the Orion association.

2. OBSERVATIONS

The targets for this study are the same 18 main-sequence stars belonging to the four subgroups of the Orion association which were analyzed in Paper I. These stars were selected from a list of members published by Warren & Hesser (1978). We restricted our sample to those members which had small projected rotational velocities ($v \sin i \leq 100$ km s^{-1}), in order to avoid line blending. The observed stars are listed in Table 1 with their spectral types, their effective temperatures ($T_{\rm eff}$), and surface gravities (g). Our choice of stellar parameters will be discussed in the next section.

[1] Observatório Nacional/CNPq, Rua General José Cristino 77, São Cristovão, Rio de Janeiro, Brazil 22921.
[2] Department of Astronomy, University of Texas, Austin, TX 78712.

TABLE 1

PROGRAM STARS AND STELLAR PARAMETERS

Star (HD)	Subgroup	Spectral Type	$T_{\rm eff}$ (K)	log g
35039	Ia	B2 V	20550	3.74
35299	Ia	B1.5V	24000	4.25
35912	Ia	B2 V	19590	4.20
36351	Ia	B1.5V	21950	4.16
36591	Ib	B1 V	26330	4.21
37744	Ib	B1.5V	24480	4.40
36285	Ic	B2 V	21930	4.40
36430	Ic	B2 V	19640	4.36
36512	Ic	B0 V	31560	4.42
36629	Ic	B2 V	22300	4.35
36959	Ic	B1 V	24890	4.41
36960	Ic	B0.5V	28920	4.33
37209	Ic	B1 V	24050	4.13
37356	Ic	B2 V	22370	4.13
37481	Ic	B1.5IV	23300	4.17
37020	Id	B0.5V	29970	3.92
37023	Id	B0.5V	32600	4.70
37042	Id	B1 V	31600	4.70

Ten spectral regions were observed with the McDonald Observatory's 2.1 m and 2.7 m telescopes and coudé spectrometers with CCD detectors. With the 2.7 m spectrometer we obtained spectra centered at 4340 Å in order to obtain the Hγ profiles from which we determine surface gravities. Nine other spectral regions observed with the 2.1 m spectrometer included a number of O II, N II, C II, Si II, Si III, and Fe III lines. The approximate central wavelengths of the observed regions were 4100, 4164, 4579, 4649, 5100, 5143, 5676, 5721, and 6387 Å. With the 2.1 m spectrometer we covered approximately 65 Å at a resolution of 0.33 Å.

The data were reduced with the IRAF data package. Our spectra have signal-to-noise ratios (S/N) in the continuum generally greater than 200, as estimated from a flat region in the spectrum. In Figure 1 we show portions of sample spectra for one of our stars for four observed wavelength regions. A total of up to 33 unblended and weak or moderately strong spectral lines were selected for measurement (Table 2). The equivalent widths of the lines were measured with the IRAF data package using a Gaussian fit and/or a straight numerical integration. For most of the lines a Gaussian fit was adequate, but the simple integration method was employed for the most rapidly rotating stars.

Our equivalent width measurements appear in Table 2. An entry consisting of a dash in the table indicates that no measurement is available because the line is either blended or very weak or not present in the spectrum. An asterisk indicates that the wavelength region that contains the line was not observed for a given star. For several stars in common, our equivalent width measurements may be compared with those obtained from Reticon spectra by Gies & Lambert (1992, hereafter GL) and from CCD spectra by Kilian & Nissen (1989, hereafter KN). The comparison is shown in Figure 2. We have excluded from the comparison with KN those lines with wavelengths between 4000 and 4200 Å because these were mentioned in their paper as being in a region where there were bad columns in their CCD. Our measurements agree well with those of GL (*filled circles*), with a tendency for their equivalent widths to be systematically smaller than ours: $W_\lambda(\mathrm{GL}) = 0.97 W_\lambda(\mathrm{CL}) - 0.86$, where CL denotes the present paper. On the other hand, KN's measurements (*filled squares*) are approximately offset from ours by a constant value: $W_\lambda(\mathrm{CL}) = W_\lambda(\mathrm{KN}) - 10$ mÅ. This trend was also noticed by GL and may reflect the fact that KN's spectra had a lower signal-to-noise ratio than our spectra.

3. ANALYSIS

The following basic steps must be completed in order to derive stellar abundances: selection of lines, measurement of equivalent widths, adoption of *gf*-values for the selected transitions, derivation of effective temperatures and gravities for the stars, and selection of appropriate model atmospheres for the derived stellar parameters. The abundances of the elements may then be calculated using the simplifying assumption that LTE is valid, or this assumption may be dropped in favor of the more realistic assumption of steady state statistical equilibrium (NLTE).

3.1. *Line Selection*

The observed spectral regions were selected on the basis of line lists compiled by Aller & Jugaku (1958) for the B star γ Peg, for a wavelength interval from about 4000 to 6000 Å, and by Kilian, Montenbruck, & Nissen (1991b) for the wavelength region between 4000 and 5000 Å.

All the lines present in our spectra were identified. These lines were examined for potential blending lines by means of

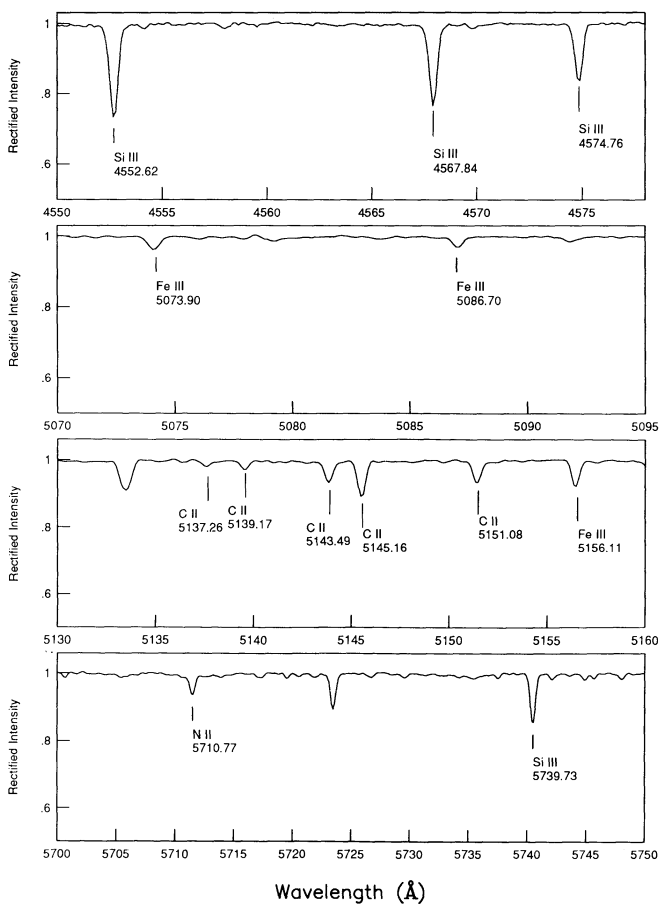

FIG. 1.—Spectrum of HD 35299 from 4550 to 4580 Å, 5070 to 5095 Å, 5130 to 5160 Å, and 5700 to 5750 Å is shown, to illustrate sample measured spectral lines. Measured C II, N II, Si III, and Fe III lines are identified.

TABLE 2

EQUIVALENT WIDTH MEASUREMENTS (mÅ)

Line	HD 35039	HD 35299	HD 35912	HD 36351	HD 36591	HD 37744	HD 36285	HD 36430	HD 36512	HD 36629	HD 36959	HD 36960
C II λ5137.3	9	9	–	7	7	–	9	–	–	9	8	–
C II λ5139.2	14	14	8	11	11	–	14	–	–	11	12	–
C II λ5143.5	34	34	21	27	24	317	31	23	–	28	27	22
C II λ5145.2	59	54	37	43	45	–	51	37	–	49	51	40
C II λ5151.1	35	36	24	27	29	30	34	–	–	34	31	31
C II λ5648.1	19	19	12	21	–	–	11	11	–	18	19	–
C II λ5662.5	27	28	17	26	21	26	29	15	–	21	25	17
N II λ4601.5	38	50	21	37	41	–	35	–	–	29	47	–
N II λ4607.2	32	40	17	32	36	42	31	18	–	26	37	20
N II λ4630.5	61	73	37	66	70	82	60	31	28	53	71	50
N II λ4643.1	36	46	19	37	38	51	36	19	–	32	41	22
N II λ5666.6	41	55	18	50	56	48	42	16	–	27	56	32
N II λ5676.0	29	40	12	36	46	38	29	17	–	21	46	26
N II λ5679.6	66	79	31	76	86	80	57	26	–	43	83	62
N II λ5686.2	21	29	–	–	37	–	18	9	–	17	31	17
N II λ5710.8	24	21	11	29	30	32	20	*	–	16	30	19
Si II λ4128.1	45	25	60	28	10	20	46	67	–	48	22	–
Si II λ4130.9	52	26	55	28	11	24	53	54	–	42	26	–
Si II λ6347.1	79	42	103	40	–	29	62	80	–	75	18	–
Si II λ6371.4	48	23	72	27	–	16	42	57	–	50	7	–
Si III λ4552.7	129	137	85	134	169	145	112	76	119	83	143	209
Si III λ4567.9	104	116	62	113	149	124	85	53	104	64	123	177
Si III λ4574.8	66	79	37	73	105	83	60	35	52	44	86	113
Si III λ5739.8	74	79	34	78	111	94	56	*	51	42	99	121
Fe III λ4081.0	13	16	–	–	19	–	11	–	–	–	18	14
Fe III λ4137.8	16	21	*	12	22	*	18	8	*	*	21	17
Fe III λ4139.4	12	20	*	–	16	*	–	–	*	*	17	–
Fe III λ4155.0	8	11	–	3	15	–	–	–	–	–	*	–
Fe III λ4166.1	12	24	12	14	37	–	–	–	9	*	*	21
Fe III λ4310.4	16	18	8	12	24	20	15	7	0	–	26	16
Fe III λ5073.9	27	23	16	17	24	22	17	10	–	13	21	–
Fe III λ5086.7	24	16	13	12	18	–	16	10	–	15	–	–
Fe III λ5156.1	38	38	28	28	41	36	33	27	–	26	41	24

TABLE 2—*Continued*

Line	HD 37209	HD 37356	HD 37481	HD 37020	HD 37023	HD 37042
C II λ5137.3	–	11	–	–	–	–
C II λ5139.2	–	14	–	–	–	6
C II λ5143.5	29	34	–	–	–	–
C II λ5145.2	51	58	–	30	–	34
C II λ5151.1	34	38	35	19	–	21
C II λ5648.1	–	22	–	–	–	–
C II λ5662.5	19	30	–	–	–	16
N II λ4601.5	–	44	–	–	–	–
N II λ4607.2	38	38	30	17	–	34
N II λ4630.5	78	72	70	–	–	–
N II λ4643.1	40	40	40	–	–	26
N II λ5666.6	54	47	59	30	–	49
N II λ5676.0	44	36	38	22	–	41
N II λ5679.6	87	73	83	49	–	71
N II λ5686.2	–	–	–	–	–	23
N II λ5710.8	29	27	30	–	–	25
Si II λ4128.1	–	33	–	–	–	–
Si II λ4130.9	–	26	–	–	–	–
Si II λ6347.1	–	48	–	–	–	–
Si II λ6371.4	–	26	–	–	–	–
Si III λ4552.7	158	109	133	131	97	150
Si III λ4567.9	118	88	107	103	96	135
Si III λ4574.8	107	60	87	64	54	86
Si III λ5739.8	87	62	66	59	54	103
Fe III λ4081.0	–	–	–	–	–	–
Fe III λ4137.8	–	15	*	–	–	*
Fe III λ4139.4	–	–	*	–	–	*
Fe III λ4155.0	–	–	*	–	–	*
Fe III λ4166.1	–	–	*	–	–	*
Fe III λ4310.4	16	11	–	–	–	21
Fe III λ5073.9	30	15	–	–	–	*
Fe III λ5086.7	29	11	–	–	–	*
Fe III λ5156.1	39	28	45	–	–	*

the line list of Kurucz & Peytremann (1975). Seriously blended lines were rejected. A total of 33 lines of C II, N II, Si II, Si III, and Fe III were selected for analysis (Table 2).

3.2. *Stellar Parameters*

One of the fundamental steps in an abundance analysis is the derivation of the stellar parameters for the generation of an appropriate model atmosphere. Our approach for deriving effective temperatures and gravities for the studied stars is similar to the one described in Gies & Lambert (1992).

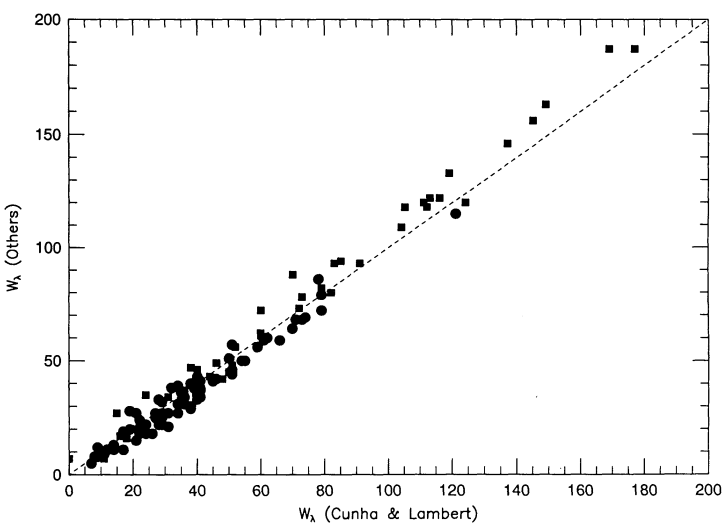

FIG. 2.—Comparison of our measured equivalent widths (in mÅ) with those of Gies & Lambert (1992) (*circles*) and Kilian & Nissen (1989) (*squares*). The dashed line illustrates the line of perfect agreement.

We make use of the calibrations of Strömgen photometry coupled with the fits to the pressure-broadened line wings of Hγ profiles in order to derive $T_{\rm eff}$ and log g. Although the Balmer jump is primarily a temperature indicator, there is some dependence on gravity, and, in addition, the line profile of Hγ is a gravity indicator but with a temperature dependence. Therefore, we employ an iterative scheme to be able to determine both $T_{\rm eff}$ and log g.

Iteration began with $T_{\rm eff}$ and log g taken from calibrations of Strömgren photometry by Lester, Gray, & Kurucz (1986, hereafter LGK) and Balona (1984). Effective temperatures from these calibrations were adjusted upward by 4.2% and 5.2%, respectively. Here we followed Gies & Lambert (1992), who found that LGK $T_{\rm eff}$ calibration needed to be increased by about 4% and Balona's temperatures by about 5% in order to make the derived temperatures consistent with the fundamental values of temperatures in Code et al. (1976). Gies & Lambert (1992) used eight stars as calibrators from the list of 32 stars presented by Code et al. (1976). They considered the stars with spectral types B3 and earlier, excluding the supergiants, and obtained for their iterative solutions estimates of log g from the literature. They calculated $T_{\rm eff}$ from the known log g by means of Balona's formula for the dereddened color index c_0. These calculations led to the revised $T_{\rm eff}$ mentioned above. We used the average of these derived temperatures from LGK and Balona in order to construct a grid of Hγ line profiles from the tabular data in Kurucz's (1979) grid. The best fit to the observed profile was found from the difference

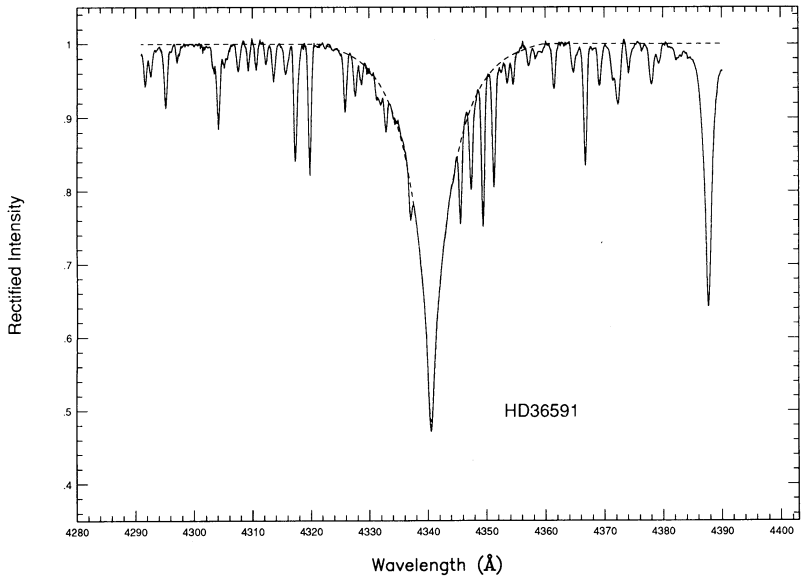

FIG. 3.—Observed spectrum of HD 36591 in the region of Hγ. The solid line represents the observed spectrum, while the dashed line shows the theoretical Hγ profile.

(minimum χ^2) between the model and the observed line profile. With this new estimate of log g, a new $T_{\rm eff}$ was derived, which was then used to construct a new grid of Hγ line profiles, so that a new log g was determined. We repeated this procedure until we obtained a consistent $T_{\rm eff}$ to within 50 K. The theoretical model profiles were broadened to include the effects of rotation, macroturbulence, and resolution. The central 3 Å of the profiles were omitted from the calculations, so that the NLTE effects in the line core would be avoided. The Hγ profile fitted for one of the studied stars is shown in Figure 3. Our derived values of $T_{\rm eff}$ and log g are listed in Table 1.

Napiwotzki, Schönberner, & Wenske (1993, hereafter NSW) have presented a thorough reexamination of the effective temperatures and surface gravities of B, A, and F stars using Strömgren photometry and Hγ line profiles. The defining $T_{\rm eff}$'s were computed for those stars with reliable measurements of their total integrated flux and accurate angular diameter measurements obtained either from the Narrabi intensity interferometer (Hanbury Brown, Davis, & Allen 1974), or indirectly from a variant of the infrared flux method. Thirty-three normal stars were available as calibrators, but only five were hotter than 20,000 K. Surface gravities from fits to Hγ profiles were checked against two stars in binary systems (α CMa and AR Aur) with well-determined gravities from the binary orbits.

NSW confirm that the Balona and LGK calibrations yield values of $T_{\rm eff}$ that are too low for hot stars. For example, NSW find $T_{\rm eff}({\rm NSW}) = (1.1 \pm 0.05)T_{\rm eff}({\rm LGK})$ for the five stars with $T_{\rm eff} > 20{,}000$ K; there is a hint that the difference between $T_{\rm eff}$(NSW) and $T_{\rm eff}$(LGK) increases with increasingly $T_{\rm eff}$. For the Balona calibration $T_{\rm eff}({\rm NSW}) = (1.07 \pm 0.5)T_{\rm eff}({\rm Balona})$. The sense of these corrections is the same as those noted by Gies & Lambert (1992) and adopted here. The corrections are slightly larger, as provided by NSW.

NSW recommended a modified form of a photometric calibration provided by Moon & Dworetsky (1985, hereafter MD; see also Moon 1985) from synthetic *uvbyβ* indices computed from Kurucz's (1979) models. The indices were adjusted to fit the $T_{\rm eff}$ and g of a few calibrating stars. In Figure 4 we show a plot of our derived effective temperatures against the results obtained from NSW's improved codes for the MD calibration (*open circles*): our temperatures are hotter than the ones based on the MD calibration by an almost constant offset of 420 K. Such a difference represents about 2.1% at the cool temperature end and about 1.4% difference at the hot end, which is within the size of the expected systematic errors of our temperature determinations (discussed in § 3.2.2).

A comparison of our derived gravities with the ones derived with NSW's values is shown in Figure 5. The average differences between log g(this paper) and log g(MD) is only 0.03 dex, and the standard deviation of the differences is 0.11 dex.

Another check of our derived stellar parameters is against the spectroscopic determinations by Kilian et al. (1991a), who derived the stellar parameters for seven stars in common with our list. Their determination of stellar parameters was based on the comparison of theoretical hydrogen line profiles with the observed spectra along with He and Si equivalent width ratios. Synthetic profiles of the hydrogen lines were computed using a NLTE line formation code (Herrero 1987) and LTE line-blanketed model atmospheres (Gold 1984). The synthetic NLTE silicon spectra generated by Becker & Butler (1990a) were used, and NLTE line formation calculations of He I and He II were carried out. Since the hydrogen line wings in B stars show a pronounced gravity dependence, and the silicon and helium lines vary more strongly with temperature, the information obtained from the hydrogen line fit is combined with that from the silicon and helium lines to fix the values of temperature and gravity.

In Figure 4 the open triangles represent the comparison between our derived temperatures and those by Kilian et al. (1991a). We find that, for the stars we have in common, Kilian et al.'s (1991a) temperatures are systematically hotter than ours; the average temperature difference is about 1000 K. Kilian et al. (1991a) compared their temperatures with the LGK calibration and found that their temperatures were also significantly hotter than the ones in LGK. They assumed that the differences between the two calibrations were due to the NLTE effects that they took into account. Napiwotzki, Schönberner, & Wenske (1992) compared Kilian et al.'s temperatures with

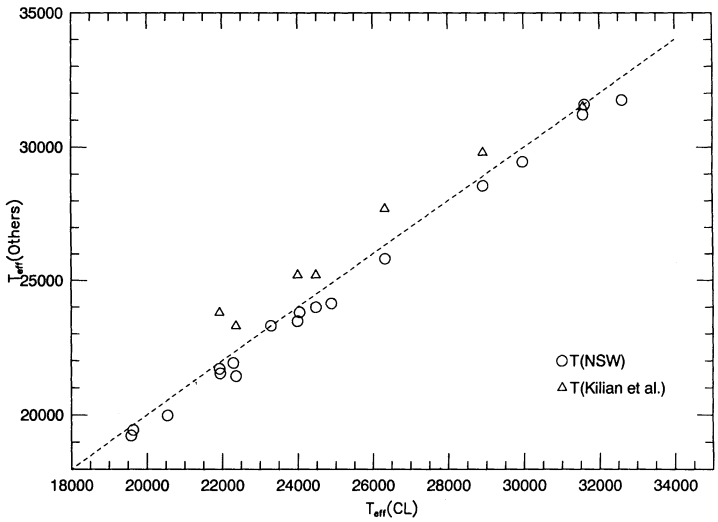

FIG. 4.—Comparison of our derived T_{eff} with those of Napiwotzki, Schönberner, & Wenske (1993) (*circles*) and Kilian et al. (1991a) (*triangles*). The dashed line shows the line of perfect agreement.

the MD temperature scale and found differences between them as large as 2000 K for the stars with temperatures around 20,000 K, but found that, on the other hand, the differences were smaller for hotter stars (around 30,000 K). We also find that the hottest star (HD 36512) we have in common with Kilian et al. (1991a) is the one that presents the smallest temperature difference [$\delta T_{eff} = T_{eff}(\mathrm{KBGN}) - T_{eff}(\mathrm{CL}) \simeq 50$ K], while the coolest star (HD 36285) we have in common gives $\delta T_{eff} = 1900$ K. This trend of δT_{eff} with temperature is illustrated in Figure 6. We suggest that the differences between the two temperature scales are not entirely due to NLTE effects; the published calculations (see below) show these effects to be more important near 30,000 K than at temperatures of the order of 20,000 K. We guess that the differences between the temperatures could be due to differences between the two families of LTE model atmospheres used: Gold's (1984) and Kurucz's (1979). This opinion is echoed by Napiwotzki et al. (1992), who recommend the use of "fully" blanketed model atmospheres like Kurucz's (1979). Kilian et al.'s (1991a) temperature are based on Gold's atmospheres, which are not fully blanketed, including only about 100 metallic lines. Line blanketing is much more fully accounted for in Kurucz's models. We later discuss in more detail the effects on the abundance analysis of the Gold and Kurucz's models.

3.2.1. *Effect of Rotation on T_{eff} and* log *g*

Our derivations of the stellar parameters have been based in nonrotating stellar models and therefore completely disregarded any changes in the structure of the stars due to stellar rotation. Although our sample of B stars consists primarily of apparently slow rotators, it may be that we are looking at the stars nearly pole-on ($i = 0°$) and it is therefore of interest to investigate the magnitude of the effect of rotation on the derived values of T_{eff} and log g for the stars.

Predicted changes in the structure of rotating stars and their effects on observable parameters have been discussed in the

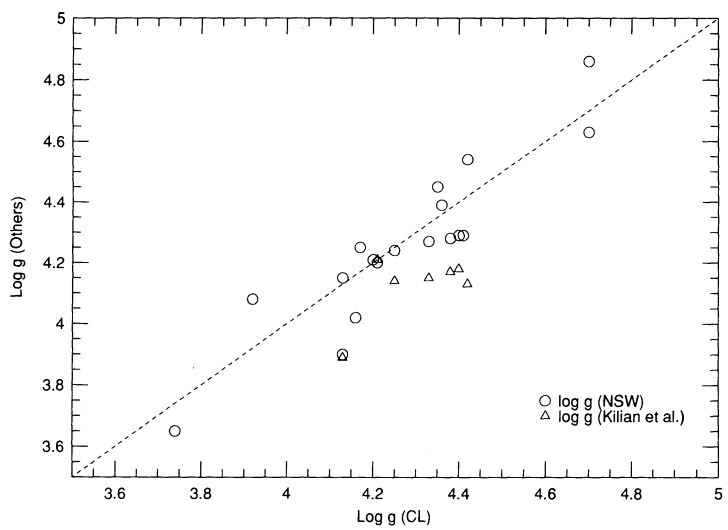

FIG. 5.—Comparison of our derived log g values with those of Napiwotzki et al. (1993) (*circles*) and Kilian et al. (1991a) (*triangles*). Note that there is no apparent trend—just random scatter about the 45° dashed line.

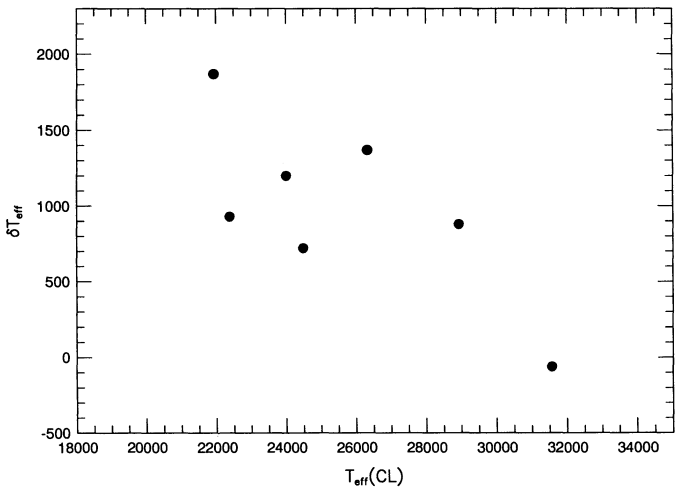

FIG. 6.—Difference between Kilian et al.'s (1991a) and our effective temperatures as a function of the star's effective temperatures, for the seven stars we have in common.

literature (see, e.g., Collins 1970). Collins, Truax, & Cranmer (1991) have presented the results of extensive model atmosphere calculations applicable to rotating early-type stars, taking into consideration the effect of line blanketing in the ultraviolet. An earlier work by Collins & Sonneborn (1977) had not included blanketing and predicted quite different theoretical colors. We have used the predictions by Collins et al. (1991) in order to investigate the effect of rotation, and we have estimated a theoretical index c_1 from their predicted theoretical indices for inclinations $i = 0°$, 45°, 60°, and 90° for a nonrotating B1 star (which corresponds to $W = 0.0$, where W is the ratio of the rotational velocity to the breakup velocity); a B1 star rotating with fractional velocities of $W = 0.5$, $W = 0.8$, and $W = 0.9$; and a critically rotating B1 star ($W = 1.0$) (Table 3). Also shown in Table 3 are the rotational velocities v. We see from Table 3 that the predicted changes in the c_1 index are about 0.01 mag for $W = 0.5$ for stars viewed equator-on ($i = 90°$) and pole-on ($i = 0°$). This difference can be as large as 0.05 mag for $W = 0.9$. In order to estimate the change in the c_1 index expected for Orion B stars due to rotation, we need to know the distribution of observed v sin i so that a typical W parameter can be selected. McNamara & Larsson (1962) have derived v sin i values for 50 B0–B3 stars in the Orion association and found an unusually high percentage of these stars to be slow rotators, with an average rotational velocity (assuming a random orientation of their axes of rotation) of 135 km s^{-1}, as compared to the mean value of 186 km s^{-1} for similar stars in the general field (Slettebak & Howard 1955). Fifty percent of the Orion stars had projected rotational velocities smaller than 50 km s^{-1}. This result has been confirmed by Abt (1970), who

TABLE 3

THEORETICAL PREDICTIONS FOR c_1

W	$i = 0°$	$i = 30°$	$i = 45°$	$i = 60°$	$i = 90°$	v (km s^{-1})
0.0.....	...	...	...	−0.058	...	...
0.5.....	−0.056	−0.051	−0.047	−0.044	−0.042	170
0.8.....	−0.05	−0.039	−0.032	−0.024	−0.015	300
0.9.....	−0.043	−0.031	−0.019	−0.006	0.01	360
1.0.....	−0.009	−0.002	0.006	0.026	−0.01	490

studied the rotational velocities of 26 early-type Orion stars and found unusually low mean rotational velocities for stars with spectral types B0–B1 compared to field stars. These results suggest that a typical B1 star in the Orion association will be rotating with a fractional velocity $W \leq 0.5$, for an assumed equatorial velocity of 170 km s^{-1}. At $W \leq 0.5$ the expected change in the photometric indices due to rotation is close to the photometric errors (0.01 mag): an uncertainty of 0.01 mag in the c_1 index will introduce an error of about 270 K (or 1.3%) in the effective temperatures for $T_{eff} = 20{,}000$ K, and an error of about 830 K (or 2.6%) for $T_{eff} = 30{,}000$ K. The log g values are reasonably insensitive to the c_1 index. Such uncertainties in the stellar parameters are then of the order of other expected uncertainties, which are discussed in the next section.

In order to evaluate fully the effect of rotation on our derived stellar parameters, we have also to consider the changes in the Hγ profiles due to stellar rotation. Collins et al. (1991) show that the wings of the Balmer lines (including Hγ) are relatively invariant to rotation even for the most rapidly rotating main-sequence models and that nearly all the rotationally induced changes in the equivalent width of lines result from changes in the line core, which are disregarded in our fits of the Hγ profiles.

The effects of stellar axial rotation on the intrinsic photometric indices of the *uvbyβ* systems have also been investigated for the B-type star members of the Orion association by Warren (1976). His paper is based on the photometric data obtained by the author at the Kitt Peak National Observatory and on v sin i values from the literature, and it is shown that no effects of rotation are present for stars with v sin $i \leq 250$ km s^{-1}. This lack of observable changes in the photometric indices agrees with the above discussion concerning the predicted effects on the *uvbyβ* indices from the theoretical models of Collins et al. (1991) and the observed distribution of v sin i in the Orion association B stars.

3.2.2. *Uncertainties in T_{eff} and* log g: *A Summary*

Our derived values of stellar parameters are subject to different sources of errors which will lead to uncertainties in our final abundances. Before turning to the next section, we summarize the sources and magnitudes of these uncertainties. This summary is in two parts: (1) those uncertainties coming from measurement errors in the photometric indices, as well as the effect of rotation on these indices, and (2) the uncertainties due to differences in the various T_{eff} and log g scales.

Errors affecting the derived values of T_{eff} and log g are contributed by the observational measurements of the Strömgren indices and Hγ profiles. As discussed in Paper I, the errors in the measured Strömgren indices are about 0.01 mag, with the exception of three stars (HD 37023, HD 37042, and HD 37481), for which the uncertainties are considered to be of the order of 0.02 mag. Another source of uncertainty for the measured indices comes from the assumption of a normal reddening law for Orion, which is used to deredden the colors. We demonstrated in Paper I that this assumption is likely to impart an error in the measured c_1 index of at most 0.01 mag. Thus, the combination of the observational uncertainties will lead to errors in the true photometric Strömgren indices of about 0.01–0.02 mag. As discussed above, the use of nonrotating stellar models for the derivation of the stellar parameters can cause changes of roughly 0.01 mag (at most) in the Strömgren indices, which will lead to a temperature uncertainty of ±1.3% (for $T_{eff} = 20{,}000$ K) and of 2.6% (for $T_{eff} = 30{,}000$ K).

Our $T_{\rm eff}$ and log g determinations also suffer from uncertainties due to systematic errors related to the $T_{\rm eff}$ scale and to the adopted line-broadening theory. We believe that the line-broadening theory should not represent a major source of uncertainty, since Kurucz (1979) tested his theoretical Hγ profiles against observations of Vega, and NSW checked their derived surface gravities against two stars for which gravities were determined from analysis of orbital motion (Habets & Heintze 1981). In order to estimate the magnitude of the systematic uncertainties in the $T_{\rm eff}$ scale, we calculated $T_{\rm eff}$ and log g for our program stars, by means of NSW's codes for MD calibrations. We note, however, that NSW's calibration does not represent a completely independent check on our derived parameters, as both are partially based on Code et al.'s (1976) standard stars and Kurucz's (1979) model atmospheres. The resulting temperatures differ from our estimated temperatures by about 2.1% for $T_{\rm eff}$ = 20,000 K and by about 1.4% for $T_{\rm eff}$ = 30,000 K.

Therefore, with observational uncertainties of about 0.01 mag, plus rotational effects of near 0.01 mag, the combined uncertainty is 0.014 mag and corresponds to an uncertainty in $T_{\rm eff}$ of 1.3% at 20,000 K and 2.6% at 30,000 K. Combined with systematic uncertainties of 2.1% (20,000 K) and 1.4% (30,000 K), a total combined estimate of the uncertainties would be 2.5% at 20,000 K and 3.0% at 30,000 K, or $\pm$500 K and $\pm$900 K, respectively, at the $T_{\rm eff}$ extremes.

The major source of uncertainty in the derivation of log g is, apart from systematic errors arising from the theory of line broadening, the placement of the continuum. We estimate that the measurement errors in the determinations are of the order of $\pm$0.1 dex. A comparison of our derived surface gravities with the ones derived with NSW's code (which are based on the same line-broadening theory) results in a mean difference in the log g values of 0.03 with a standard deviation of 0.11, identical, for all purposes, with our error estimates.

3.3. *LTE Abundances: Method*

The effective temperatures and gravities discussed in the last section were used to generate line-blanketed model atmospheres using the ATLAS6 code (Kurucz 1979), assuming a solar composition and a depth-independent microturbulent velocity of 2 km s^{-1}. These model atmospheres were part of the input to the program WIDTH6 (R. L. Kurucz 1990, private communication), which was used to derive the abundances. Other input data include the gf-values of individual lines and the microturbulence. Our abundances are quite insensitive to the adopted damping constants which were obtained from Kilian et al. (1991b).

3.3.1. *The gf-Values*

The gf-values of the lines used in the abundance calculations are presented in Table 4 for C, N, Si, and Fe lines. The gf-values used for O II lines are listed in Paper I. The gf-values for the C II multiplets were obtained from the Opacity Project (OP) calculations database (A. K. Pradhan & S. Nahar 1992, private communication). In general, OP gf-values are believed to be accurate to within 10% except when the radial integrals are subject to severe cancellation (Seaton et al. 1993). For N II lines, we obtained the multiplet gf-values from Becker & Butler (1989), which are also believed to be accurate to about 10%. For C II and N II lines, we computed the multiplet gf-values assuming that their relative line strengths are the values appropriate for LS coupling. For Si II and Si III lines, the gf-values were directly obtained from Becker & Butler (1990a) except for three of the lines (indicated wih a superscript "a" in Table 4), for which the Kurucz & Peytremann (1975, hereafter KP) values have been employed, since more recent values were not available.

TABLE 4

THE TRANSITIONS

Line	Multiplet	J	χ	log gf
C II λ5137.257	$3s\,^4P^o$–$3p\,^4P$	0.5–0.5	20.70	−0.912
C II λ5139.174		1.5–1.5	20.70	−0.707
C II λ5143.494		1.5–0.5	20.70	−0.213
C II λ5145.165		2.5–2.5	20.71	0.189
C II λ5151.085		2.5–1.5	20.71	−0.179
C II λ5648.070	$3s\,^4P^o$–$3p\,^4S$	1.5–1.5	20.70	−0.421
C II λ5662.460		2.5–1.5	20.71	−0.245
N II λ4601.478	$3s\,^3P^o$–$3p\,^3P$	1–0	18.47	−0.384
N II λ4607.153		0–1	18.46	−0.482
N II λ4630.540		2–2	18.46	0.092
N II λ4643.086		2–1	18.48	−0.387
N II λ5666.629	$3s\,^3P^o$–$3p\,^3D$	1–2	18.47	−0.044
N II λ5676.017		0–1	18.46	−0.396
N II λ5679.558		2–3	18.48	0.227
N II λ5686.212		1–1	18.47	−0.521
N II λ5710.766		2–2	18.48	−0.521
Si II λ4128.053	$3d\,^2D$–$4f\,^2F^o$	1.5–2.5	9.84	−0.029
Si II λ4130.872		2.5–2.5	9.84	0.323
Si II λ6347.109	$4s\,^2S$–$4p\,^2P^o$	0.5–1.5	8.12	0.23[a]
Si II λ6371.372		0.5–0.5	8.12	−0.07[a]
Si III λ4552.622	$4s\,^3S$–$4p\,^3P^o$	1–2	19.02	0.283
Si III λ4567.841		1–1	19.02	0.06
Si III λ4574.757	$4s\,^3S$–$4p\,^3P^o$	1–0	19.02	−0.417
Si III λ5739.734	$4s\,^1S$–$4p\,^1P^o$	0–1	19.72	0.050[a]
Fe III λ4081.00	$(^6S)5p\,^7P$–$(^6S)6s\,^7S$	4–3	20.63	0.38[a]
Fe III λ4137.764	$(^6S)5p\,^7P$–$(^6S)5d\,^7D$	3–4	20.61	0.65[a]
Fe III λ4139.350		3–3	20.61	0.54[a]
Fe III λ4154.963	$(^4G)5p\,^5H$–$(^4G)5d\,^5I$	5–6	24.64	0.97[a]
Fe III λ4166.840	$(^6S)5p\,^7P$–$(^6S)5d\,^7D$	4–4	20.63	0.43[a]
Fe III λ4310.355	$(^6S)4f\,^7F$–$(^6S)5g\,^7G$	6–7	22.87	1.17[a]
Fe III λ5073.903	$(^4D)4s\,^5D$–$(^6S)4p\,^5P^o$	1–1	8.65	−2.77[a]
Fe III λ5086.701		2–1	8.66	−2.78[a]
Fe III λ5156.111		4–3	8.64	−2.23[a]

[a] log gf from Kurucz & Peytremann 1975.

Opacity Project gf-values for the Fe III lines were provided by S. Nahar (1993, private communication). A comparison of these results with the KP values shows that the OP values are a surprising 1.0–1.5 dex smaller for the three multiplets originating from the $3d^5(a\,^6S)5p\,^7P^o$ level. Use of the KP gf-values leads to a reasonably consistent set of LTE Fe abundances. Adoption of the OP gf-values leads, of course, to Fe abundances spanning a range of about 1.5 dex, in contrast to the range of 0.6 dex from KP gf-values. The stellar Fe III lines suggest that either the OP gf-values for the multiplets from $3d^5(a\,^6S)5p\,^7P^o$ are in error or there are strong and selective NLTE effects.

The line-to-line spread of the Fe abundances from KP's gf-values is somewhat larger than we find for our selection of C II, N II, and O II lines. In order to minimize the effect of the uncertainties of the Fe gf-values on the abundance calculations, we derived the Fe abundances relative to a reference star (HD 35299). The differential abundances, δ log ϵ(Fe), listed in Table 5 are average values calculated from the differential abundances of the individual lines relative to HD 35299; we also list the standard deviation and the number of lines (n). The

TABLE 5

Fe Differential Abundances

Star (HD)	δ log ϵ(Fe)	n
35039	-0.03 ± 0.05	8
35299	0.00[a]	8
35912	$+0.13 \pm 0.02$	5
36351	-0.12 ± 0.02	6
36591	-0.01 ± 0.04	8
37744	-0.03 ± 0.05	4
36285	$+0.11 \pm 0.03$	6
36430	$+0.09 \pm 0.05$	5
36512	-0.15	1
36629	-0.05 ± 0.08	3
36959	$+0.06 \pm 0.04$	6
36960	-0.01 ± 0.03	5
37209	$+0.01 \pm 0.08$	4
37356	-0.16 ± 0.02	5
37481	$+0.03$	1
37020	...	...
37023	...	...
37042	$+0.28$	1

[a] Reference star.

absolute Fe abundances calculated from the KP *gf*-values are listed in Table 6. The line-to-line scatter of the differential Fe abundances is, as expected, significantly smaller than the scatter in the absolute Fe abundances; a part of the scatter found in the absolute abundances is certainly due to errors in the KP *gf*-values.

3.3.2. *Microturbulence*

A step in the determination of stellar abundances is the derivation of the microturbulence velocity for the stars. We employed the O II, N II, and Si III lines for the completion of this task. The lines of O II and N II spanned a range in equivalent widths, from weak to moderately strong lines, while the Si III lines were more concentrated toward strong lines (the most sensitive to microturbulence).

In order to derive microturbulence velocities for the LTE analysis, the program WIDTH6 was run for various values of microturbulent velocities for each star. We determined the best microturbulence as that which yielded a zero slope in a diagram of log abundance versus equivalent width. We derived the microturbulence separately for O II, N II, and Si III lines and adopted the mean microturbulence as weighted by the number of lines in each species, rounded to the nearest 0.5 km s^{-1}. Our derived values of microturbulence are listed in Table 6.

In our choice of the microturbulence, we did not consider the C II lines because the observed selection lacks strong lines. Si II lines also were not included; there are very few lines of this species for the temperatures we are considering. We elected not to consider Fe III lines because their *gf*-values are considered to be less accurate.

The uncertainties in the derived values of microturbulence are inferred to be of the order of 1.5 km s^{-1}. This value was estimated from inspection of the typical behavior of abundance versus microturbulence for the lines considered, looking for tolerable agreement between the abundances from weak and strong lines. A comparison of our microturbulences based upon the sample of O II, N II, and Si III lines with the microturbulences adopted in Paper I based exclusively on O II lines shows that the present microturbulence values tend to be smaller than the previous adopted values by roughly 1–2 km s^{-1}.

The microturbulences for the NLTE analysis were estimated in a similar way to the LTE estimates, but by means of interpolation in the equivalent width tables provided as a function of microturbulence. The derived values of microturbulent velocities are listed in Table 7. The mean difference between the NLTE and the LTE adopted microturbulences is 0.4, with a standard deviation of 1.2 km s^{-1}

3.4. *LTE Abundances: Results*

Our calculated logarithmic abundances for C, N, O, Si, and Fe, on a scale where log ϵ(H) equals 12, are presented in Table 6. The abundance values listed for the elements represent the mean stellar abundances for the calculated individual line abundances together with the corresponding standard error of the mean. The number of lines n considered in the calculation of the mean abundance values is also listed.

Carbon.—The sampled C II lines belong to two different

TABLE 6

LTE Abundances

Star (HD)	ξ (km s^{-1})	log ϵ(C)	n	log ϵ(N)	n	log ϵ(O)	n	log ϵ(Si)	n	log ϵ(Fe)	n
35039	9.0	8.39 ± 0.02	7	7.78 ± 0.02	9	8.58 ± 0.04	15	7.39 ± 0.04	4	7.41 ± 0.08	8
35299	6.5	8.34 ± 0.02	7	7.81 ± 0.02	9	8.58 ± 0.04	14	7.32 ± 0.02	4	7.44 ± 0.07	8
35912	8.0	8.39 ± 0.02	6	7.78 ± 0.03	8	8.64 ± 0.03	8	7.38 ± 0.03	4	7.65 ± 0.08	5
36351	8.0	8.31 ± 0.03	6	7.86 ± 0.04	8	8.73 ± 0.06	13	7.46 ± 0.02	4	7.36 ± 0.09	6
36591	10.0	8.31 ± 0.03	6	7.72 ± 0.03	9	8.64 ± 0.05	11	7.27 ± 0.04	4	7.44 ± 0.10	8
37744	7.5	8.30 ± 0.02	3	7.79 ± 0.03	7	8.64 ± 0.05	11	7.34 ± 0.02	4	7.43 ± 0.13	4
36285	7.0	8.41 ± 0.03	7	7.89 ± 0.02	9	8.79 ± 0.03	12	7.38 ± 0.04	4	7.56 ± 0.07	6
36430	7.0	8.43 ± 0.03	4	7.80 ± 0.04	6	8.85 ± 0.08	7	7.37 ± 0.04	3	7.56 ± 0.08	5
36512	8.0[a]	...	...	...	...	8.57 ± 0.06	11	7.33 ± 0.03	3	7.40	1
36629	5.0	8.32 ± 0.03	7	7.73 ± 0.02	8	8.57 ± 0.04	10	7.17 ± 0.03	4	7.58 ± 0.07	3
36959	5.5	8.31 ± 0.02	7	7.82 ± 0.03	9	8.88 ± 0.04	10	7.50 ± 0.03	4	7.46 ± 0.08	6
36960	8.0	8.34 ± 0.03	4	7.65 ± 0.03	7	8.76 ± 0.02	11	7.62 ± 0.04	3	7.36 ± 0.09	5
37209	10.0	8.26 ± 0.03	4	7.67 ± 0.03	7	8.73 ± 0.06	7	7.19 ± 0.08	4	7.53 ± 0.18	4
37356	7.5	8.39 ± 0.03	7	7.83 ± 0.02	8	8.65 ± 0.04	13	7.18 ± 0.02	4	7.30 ± 0.09	5
37481	9.0	8.32	1	7.72 ± 0.03	7	8.87 ± 0.08	3	7.18 ± 0.09	4	7.55	1
37020	7.0	8.33 ± 0.06	2	7.64 ± 0.05	4	8.92 ± 0.05	6	7.40 ± 0.01	3	...	...
37023	7.5[a]	...	...	...	...	8.76 ± 0.04	7	7.34 ± 0.07	4	...	...
37042	6.0	8.47 ± 0.02	4	8.09 ± 0.06	7	8.97 ± 0.04	7	7.67 ± 0.01	4	7.48	1

[a] Microturbulence derived from the O II and Si III lines.

TABLE 7

NLTE ABUNDANCES

Star (HD)	ξ (km s^{-1})	log ϵ(C)	n	log ϵ(N)	n	log ϵ(O)	n	log ϵ(Si)	n
35039	8.0	8.50 ± 0.03	7	7.85 ± 0.05	4	8.60 ± 0.04	12	7.27 ± 0.03	3
35299	8.0	8.38 ± 0.03	7	7.74 ± 0.06	4	8.57 ± 0.04	12	6.97 ± 0.04	3
35912	8.0	8.55 ± 0.03	6	7.89 ± 0.04	4	8.70 ± 0.05	7	7.28 ± 0.04	3
36351	9.0	8.35 ± 0.04	7	7.83 ± 0.03	4	8.76 ± 0.06	11	7.22 ± 0.06	3
36591	9.0	8.25 ± 0.03	6	7.58 ± 0.05	4	8.60 ± 0.05	8	6.93 ± 0.11	3
37744	7.0	8.34 ± 0.02	3	7.85 ± 0.04	3	8.63 ± 0.06	10	7.22 ± 0.09	3
36285	8.0	8.57 ± 0.04	7	7.95 ± 0.04	4	8.80 ± 0.05	10	7.20 ± 0.07	3
36430	9.0	8.54 ± 0.03	4	7.89 ± 0.09	3	8.84 ± 0.04	6	7.22 ± 0.05	3
36512	9.0	...	...	...	...	8.47 ± 0.08	9	7.10 ± 0.05	3
36629	8.0	8.38 ± 0.03	7	7.75 ± 0.03	4	8.55 ± 0.06	9	6.89 ± 0.06	3
36959	6.0	8.33 ± 0.02	7	7.76 ± 0.05	4	8.76 ± 0.06	9	7.12 ± 0.09	3
36960	8.0	8.36 ± 0.01	4	7.50 ± 0.04	3	8.72 ± 0.04	8	7.29 ± 0.05	3
37209	10.0	8.27 ± 0.04	4	7.63 ± 0.05	3	8.83 ± 0.08	7	7.05 ± 0.12	3
37356	9.0	8.46 ± 0.03	7	7.84 ± 0.04	4	8.67 ± 0.05	11	6.96 ± 0.08	3
37481	9.0	8.40	1	7.65 ± 0.02	3	8.96 ± 0.08	3	7.04 ± 0.12	3
37020	5.0	8.25 ± 0.06	2	7.69	1	8.83 ± 0.12	7	7.16 ± 0.05	3
37023	7.0	...	...	...	...	8.87 ± 0.08	6	7.18 ± 0.08	3
37042	6.0	...	...	...	...	8.85 ± 0.06	6	7.33 ± 0.08	3

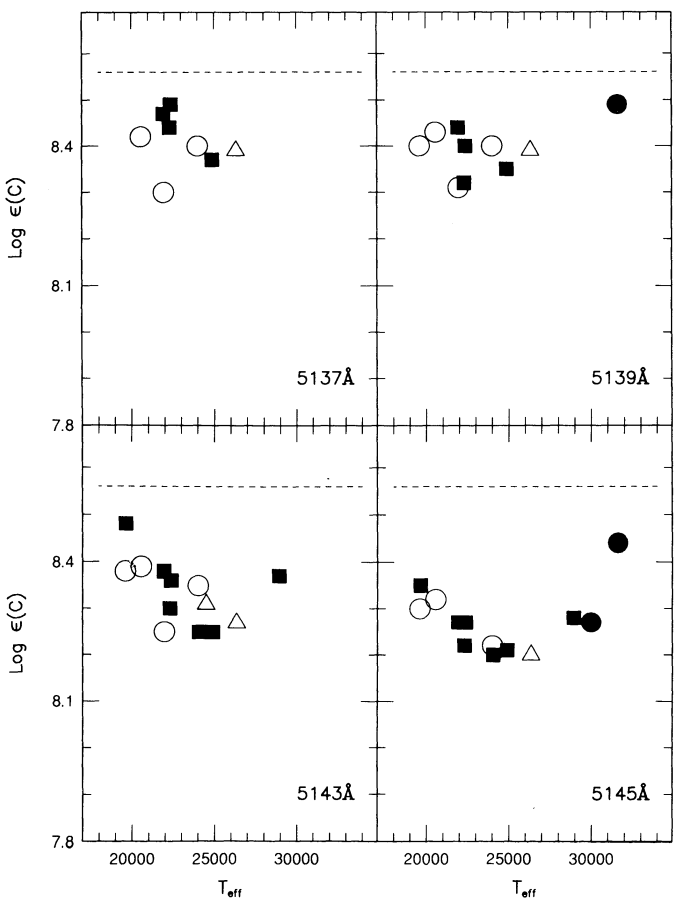

FIG. 7a

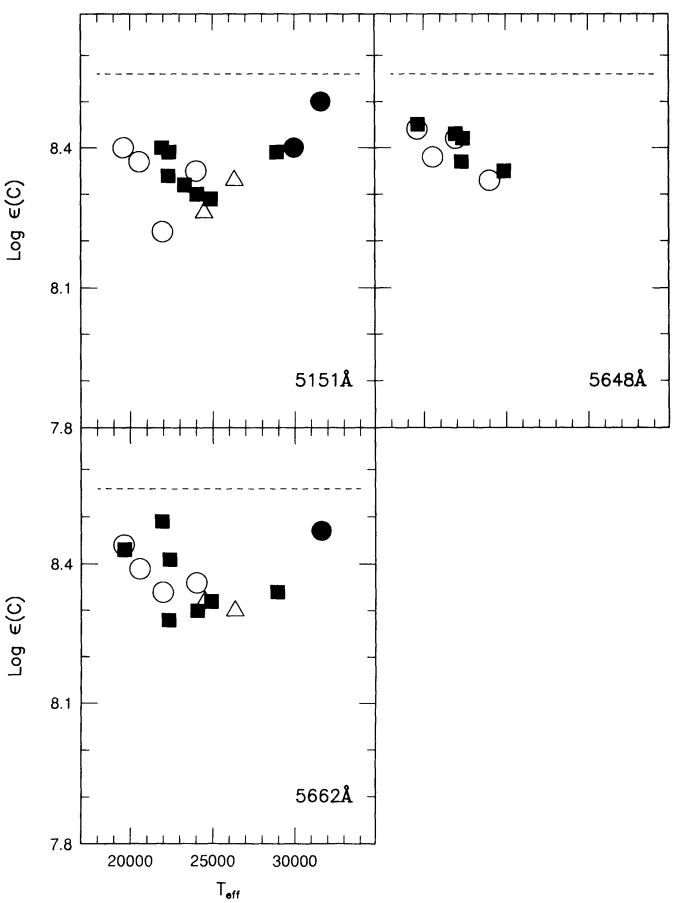

FIG. 7b

FIG. 7.—Carbon abundances from individual C II lines shown as a function of the star's effective temperatures. The lines are identified by their wavelength in the bottom right-hand corner of each panel. The open circles represent stars belonging to subgroup Ia, the open triangles to Ib, the filled squares to Ic, and the filled circles to Id. The reference (solar) abundance of log ϵ(C) = 8.56 is denoted by the dashed line.

multiplets. Abundances from individual lines of these multiplets are plotted against $T_{\rm eff}$ in Figures 7*a* and 7*b*. The two multiplets give essentially identical abundances. Mean stellar abundances shown in Figure 8 show little to no variation with $T_{\rm eff}$. The C abundance possibly reaches a minimum value at $T_{\rm eff} = 26{,}000$ K. A least-squares fit gives log ϵ(C) $= -6.09 \times 10^{-7} T_{\rm eff} + 8.37$, or the carbon abundance is increased by only 0.006 dex (a negligible quantity) as $T_{\rm eff}$ runs from 20,000 to 30,000 K. The possible errors of the adopted $T_{\rm eff}$ scale could account for part of this possible (very small) trend with $T_{\rm eff}$: for example, if the temperatures are raised by 2% (400 K at $T_{\rm eff} =$ 20,000 K, and 600 K at $T_{\rm eff} = 30{,}000$ K), the trend would be eliminated (see Table 11 for more details).

Nitrogen.—Two N II multiplets were observed and yield quite similar abundances. Abundances from two lines of each multiplet are plotted against $T_{\rm eff}$ in Figure 9. The mean nitrogen abundances may decline slightly with increasing $T_{\rm eff}$ (Fig. 8) by an amount that is slightly larger than the marginal decrease shown by the C abundances. One outstanding N-rich star (HD 37042) must be discarded in looking for a $T_{\rm eff}$-dependent trend. A decision about a trend then depends on the N abundances of the two remaining hottest stars. The error analysis reported in § 3 and Table 11 shows that the apparent trend is completely removable by adjustment of the $T_{\rm eff}$ scale within the 2% uncertainty that we assign (§ 3.2.2) to that scale.

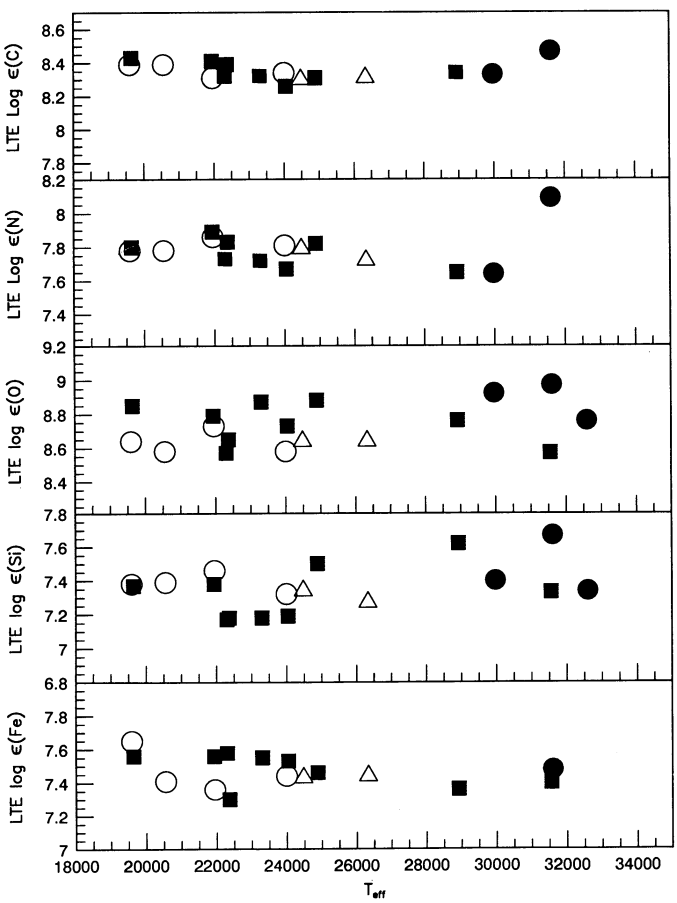

FIG. 8.—Mean LTE abundances as a function of the stars' effective temperatures. The symbols used to distinguish the four subgroups are described in Fig. 7.

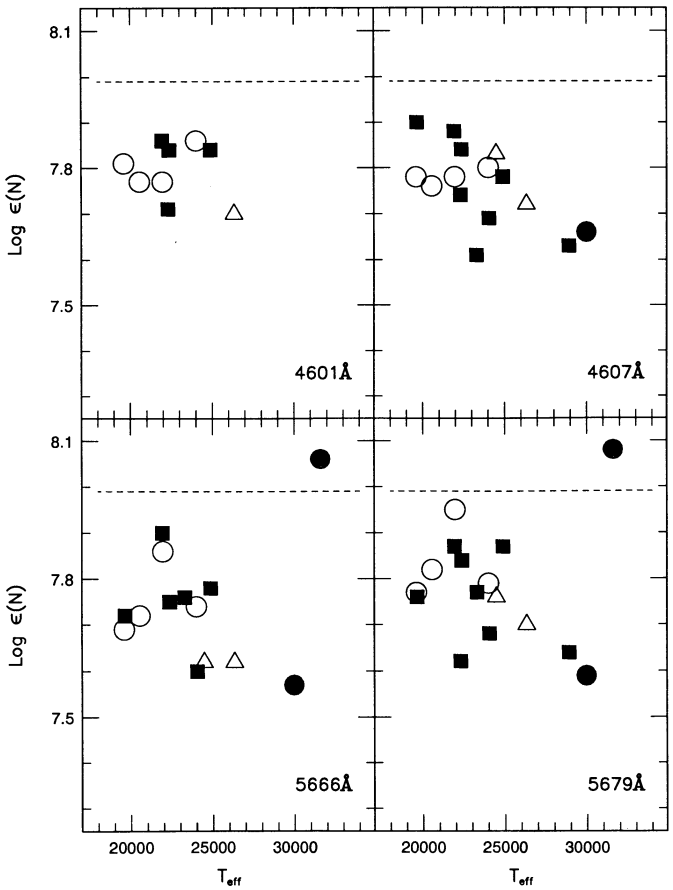

FIG. 9.—Same as Fig. 7, but for some N II lines in our sample. The reference (solar) abundance of log ϵ(N) = 8.05 is denoted by the dashed line.

Oxygen.—The O abundances are based on Paper I but have been recomputed for the new values of the microturbulence. As mentioned before, the new derived values of microturbulence tend to be smaller than the previous ones. Such a small change in the adopted microturbulence produces but a small change in the O abundances, since our selected O II lines are weak. The O abundances for the stars are listed in Table 6. The mean O abundances as a function of $T_{\rm eff}$ are presented in Figure 8. Inspection of Figure 8 shows no significant trend of the abundances with effective temperatures.

Silicon.—The Si III lines were observable in all stars, but the Si II lines were reliably detected only in the stars with $T_{\rm eff} <$ 25,000 K. Abundances from individual lines are shown in Figures 10 (Si II) and 11 (Si III). One notices immediately that the Si II lines give a significantly lower abundance than the Si III lines. The "Si II" abundance is substantially below the solar value. For the LTE silicon abundance, we adopt the Si III lines on the grounds that the Si^{2+} ions are the dominant ion over much of the $T_{\rm eff}$ range, and, hence, the derived abundances are relatively insensitive to errors in the adopted $T_{\rm eff}$ and log g. We comment further on the "Si II" and "Si III" abundances in § 3.5.1.

The mean Si abundances from Si III lines are shown in Figure 8. Viewed without consideration of subgroup membership, the Si abundances may increase with increasing $T_{\rm eff}$. Si follows O in showing a larger scatter than either C or N in the abundance at a given $T_{\rm eff}$. If the C and N trends reflect a systematic error in the $T_{\rm eff}$ scale, the correction to be applied to

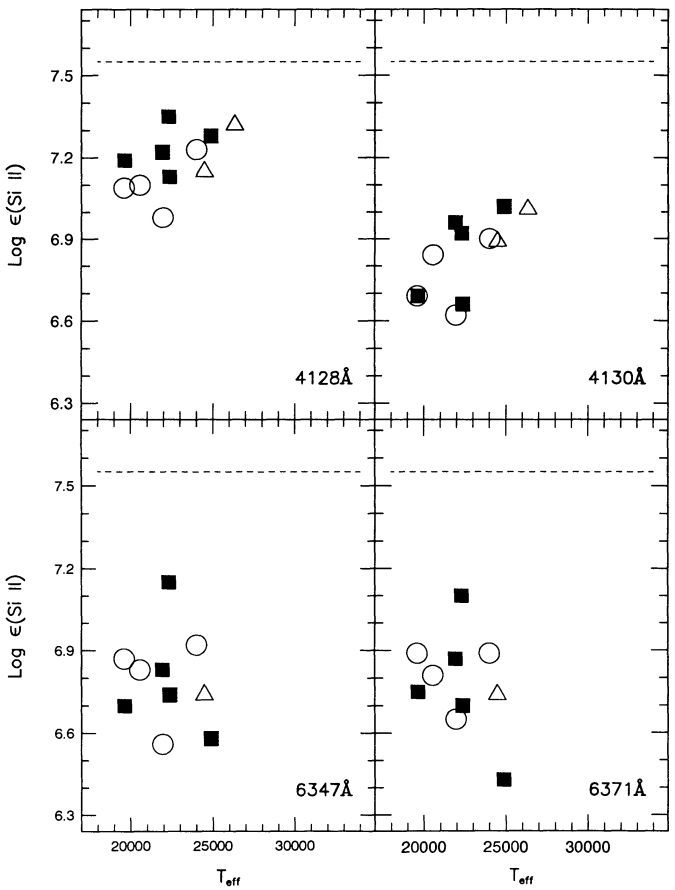

FIG. 10.—Same as Fig. 7, but for Si II lines. The reference (solar) abundance of log ϵ(Si) = 7.55 is denoted by the dashed line.

the Si abundances will enhance the apparent trend of Si to rise with T_{eff}.

Iron.—A maximum of nine Fe III lines were available; absolute abundances from this nonet are shown in Figure 12. In Table 6 we show the absolute Fe abundances calculated with the KP *gf*-values. As noted in § 3.3, the inaccuracies in the KP *gf*-values contribute significantly to the spread in the absolute abundances, and, hence, we elect to present differential abundances line by line relative to one star (HD 35299). These differential abundances are shown in Figure 13, but a trend with T_{eff}, if present, is masked by the lack of Fe abundance determinations for several of the hottest stars of the sample.

In addition to Fe, we calculated the differential abundances on a line-by-line basis for C, N, O, and Si. The scatter in the differential abundances is similar to the scatter in the absolute abundances, indicating that the errors in the *f*-values are not a major contributor to the abundance scatter.

3.5. *NLTE Abundances: Results*

Published analyses of NLTE effects on the C II, N II, O II, and Si III lines show that the NLTE abundances can differ from the LTE abundances by amounts comparable to the abundance spread across the subgroups of the Orion association. Therefore, we elected to determine the NLTE abundances from the NLTE calculations carried out by the "Munich group" for C, N, O, and Si; calculations have not been published for Fe. These calculations are based on LTE line-blanketed model atmospheres from Gold (1984) which include only the opacity of the 104 strongest metallic lines present in B stars. NLTE unblanketed models were available to the Munich group, but Gold's line-blanketed models were preferred because the effects of line blanketing were recognized as having a more important influence than NLTE effects on the atmospheric structure of B stars (Becker & Butler 1989). Kurucz's more heavily line-blanketed LTE models are now available, but detailed NLTE calculations have not been reported for such models.

Our applications of the NLTE calculations for C II, N II, Si II, and Si III are discussed next. These applications show a T_{eff}-dependent trend for the C and N abundances but not for O and Si abundances. In § 3.5.2 we suggest that this trend may be due to the use of lightly blanketed Gold models.

Due to the differences in the temperature structure in the atmospheres of Gold and Kurucz models, the temperatures for which the LTE equivalent widths of a given line of an ion reaches the maximum are lower in Kurucz's models than in Gold's models. This is illustrated in Figure 14, where we plot the behavior of the equivalent widths for the 4630 Å N II line with effective temperature.

3.5.1. *The NLTE Abundances*

Carbon.—For the C II lines we used predictions of NLTE equivalent widths as a function of effective temperature, log *g*, carbon abundance, and three different values of microturbulences (0, 5, and 10 km s^{-1}). These predictions, which

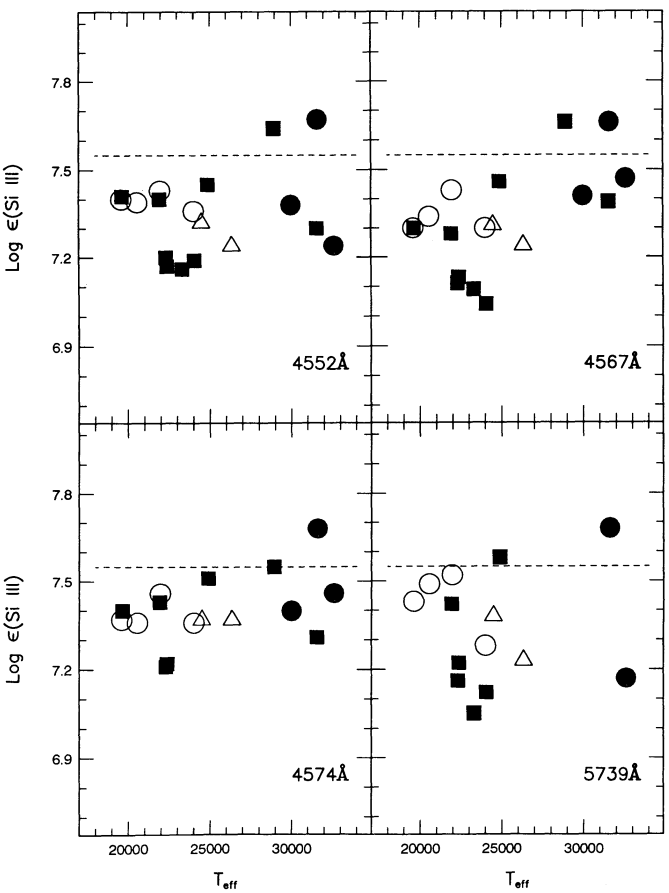

FIG. 11.—Same as Fig. 7, but for Si III lines. The reference (solar) abundance of log ϵ(Si) = 7.55 is denoted by the dashed line.

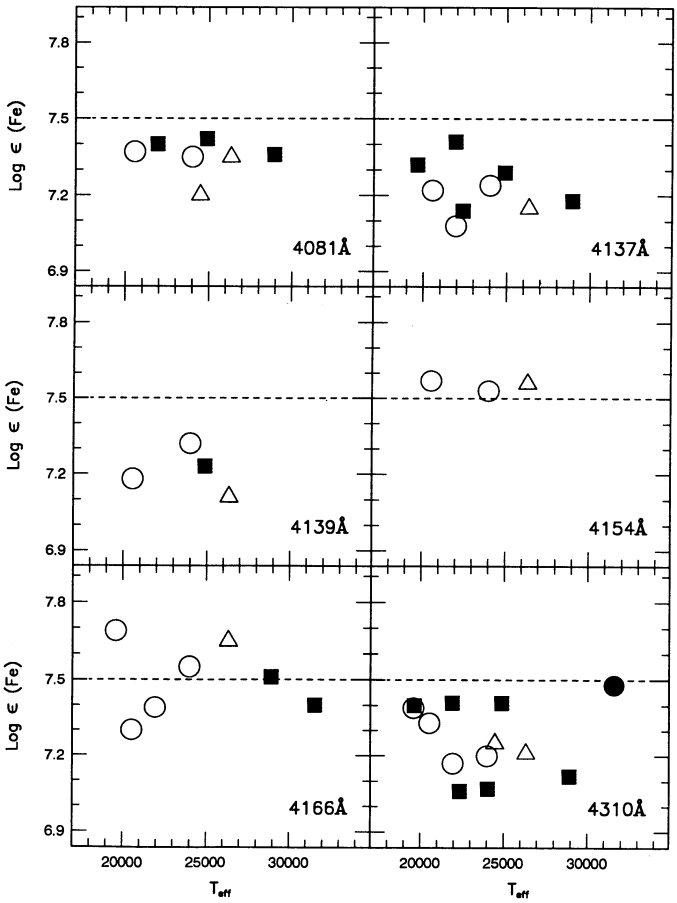

FIG. 12*a*

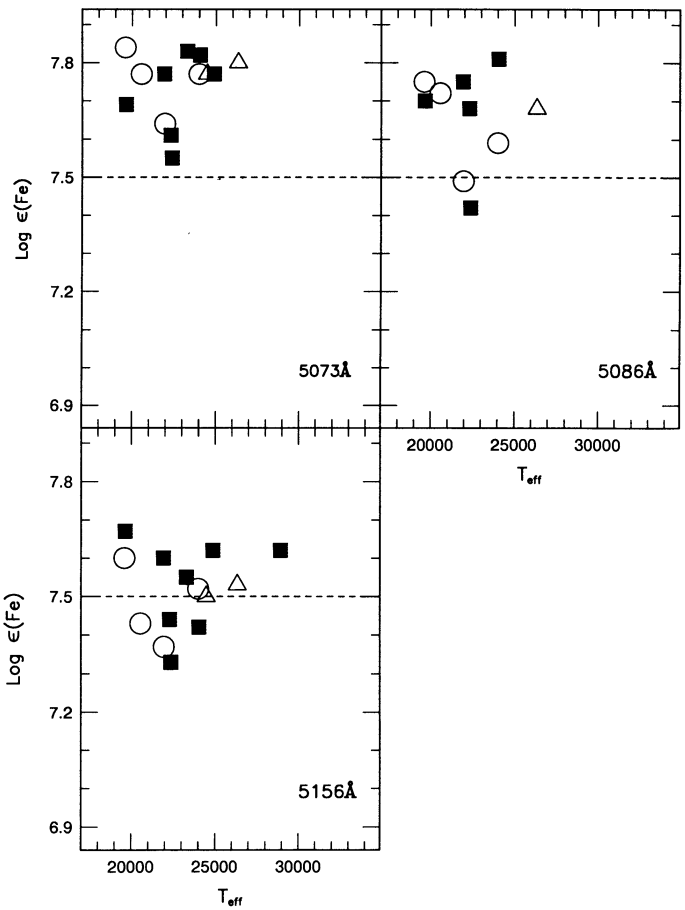

FIG. 12*b*

FIG. 12.—Same as Fig. 7, but for Fe III lines. The reference (solar) abundance of log ϵ(Fe) = 7.52 is denoted by the dashed line.

were kindly provided by S. Becker (1993, private communication), employed the extensive model atom for C II presented in Eber & Butler (1988). We estimated the NLTE carbon abundances for individual lines by interpolating in the equivalent width tables provided. The *gf*-values assumed in the prediction of the NLTE equivalent widths are identical to those adopted by us for the LTE abundances. The mean NLTE carbon abundances for the target stars together with the standard error of the mean and the number n of lines considered in the calculations are listed in Table 7.

The NLTE carbon abundances decline with increasing $T_{\rm eff}$ (see Fig. 15) from 20,000 to 26,000 K. Since the decline by

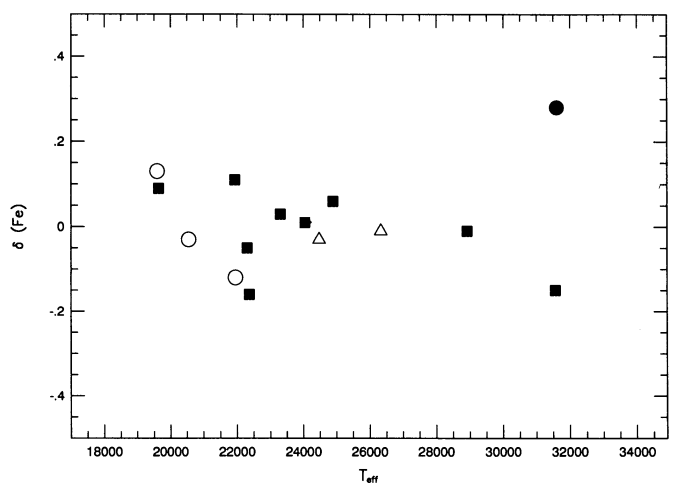

FIG. 13.—Differential iron abundances from individual Fe III lines as a function of the stars' effective temperatures. The symbols used to distinguish the four subgroups are described in Fig. 7.

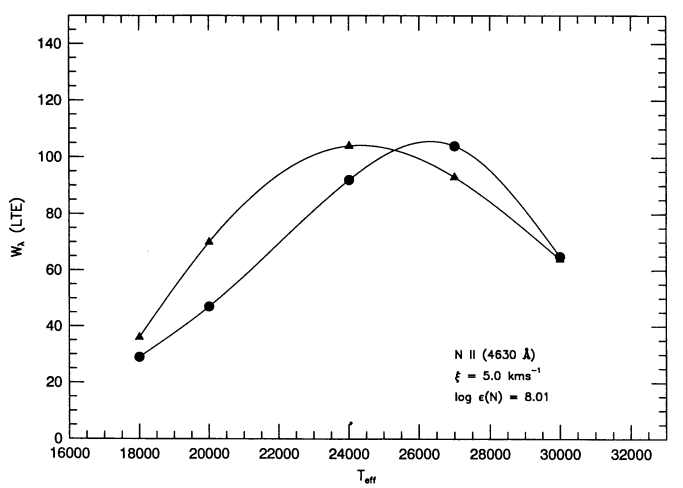

FIG. 14.—Change in the LTE equivalent width of the N II line (4630 Å) as a function of effective temperature for Kurucz's (*triangles*) and Gold's (*circles*) model atmospheres.

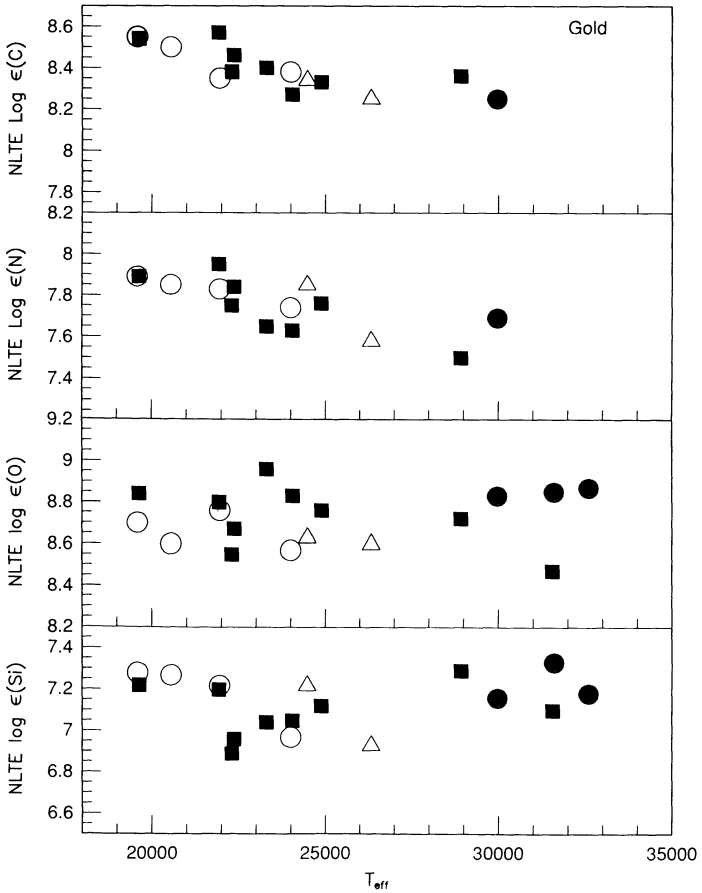

FIG. 15.—Mean NLTE carbon, nitrogen, oxygen, and silicon abundances as a function of the stars' effective temperatures. The calculations were done by means of Gold's model atmospheres. The symbols used to distinguish the four subgroups are described in Fig. 7.

about 0.3 dex exceeds that expected from likely manipulations of the T_{eff} scale, we must look for another cause (see § 3.5.2).

Nitrogen.—For the N II lines, we employed the grid of NLTE equivalent widths calculated by Becker & Butler (1988), which is based upon their extensive N II model atom (Becker & Butler 1989). Calculations for additional models and N II lines were kindly provided by S. R. Becker (1991, private communication). The NLTE N II predictions and our LTE abundance calculations use the same *gf*-values.

In Table 8 we present the LTE (Kurucz) and NLTE (Gold) abundances calculated for the individual N II lines for three values of microturbulence ($\xi = 0$, 5, and 10 km s^{-1}) for a representative star, HD 35299. Inspection of the table shows that the LTE (Kurucz) and NLTE (Gold) abundances for the lines belonging to the $3s\,^3P^o$–$3p\,^3P$ triplet (4601–4643 Å) are not very different (mean difference of 0.04 dex) but that, on the other hand, the lines belonging to the $3s\,^3P^o$–$3p\,^3D$ triplet (5666–5710 Å) show quite different LTE and NLTE abundances (mean difference of −0.35 dex). Table 8 shows that the LTE abundances are essentially identical for the two multiplets, but the NLTE abundances differ by 0.4 dex. A possible interpretation is that the NLTE calculations are presently incomplete for one or both multiplets. In order to investigate this possibility, we derived NLTE abundances for several other N II lines. The equivalent widths of three N II lines belonging to a different triplet ($3p\,^3D$–$3d\,^3D^o$ at 4779–4788 Å) were obtained from Killian & Nissen (1989) for HD 35299. The NLTE abundances (Table 9) for these three lines are in very good agreement with the NLTE abundances calculated from the $3s\,^3P^o$–$3s\,^3P$ triplet and therefore are also very different from the abundances calculated for the N II lines belonging to the $3s\,^3P^o$–$3p\,^3D$ triplet. (The LTE abundances from these three additional lines are in good agreement with the LTE abundances from the other lines.)

TABLE 8

LTE AND NLTE ABUNDANCES FOR HD 35299

N II LINE (Å)	LTE/NLTE		
	$\xi = 0.0$	$\xi = 5.0$	$\xi = 10.0$
4601.5	8.06/8.12	7.86/7.96	7.78/7.84
4607.2	7.96/8.01	7.84/7.90	7.75/7.80
4630.5	8.04/7.97	7.77/7.75	7.58/7.58
4643.1	8.00/8.00	7.85/7.87	7.75/7.75
5666.6	7.99/7.50	7.80/7.45	7.66/7.38
5676.0	8.02/7.67	7.91/7.59	7.81/7.52
5679.6	8.20/7.66	7.88/7.46	7.65/7.32
5686.2	7.87/7.57	7.82/7.52	7.76/7.47
5710.8	8.01/7.66	7.93/7.59	7.85/7.53

A comparison of the calculated NLTE equivalent widths of two N II lines, one belonging to the $3s\,^3P^o$–$3p\,^3D$ multiplet (4630.54 Å) and another belonging to the $3s\,^3P^o$–$3p\,^3P$ multiplet (5666.63 Å) shows that, at an effective temperature of 24,000 K and log $g = 4.25$, the predicted equivalent width for 4630.54 Å is smaller than the predicted equivalent width for 5666.63 Å. But this trend is opposite to the trend we observe for HD 35299 (see Table 2), which has a T_{eff} of 24,000 K and a log g of 4.25.

The variation of the calculated NLTE equivalent width with effective temperature is plotted in Figure 16 for a representative transition of the $3s\,^3P^o$–$3p\,^3P$ and $3s\,^3P^o$–$3p\,^3D$ multiplets, for log $g = 4.0$, $\xi = 5.0$ km s^{-1}, and a solar nitrogen abundance. It can be seen from this figure that W_λ(4630.54 Å) < W_λ(5666.63 Å) for effective temperatures less than roughly 27,000 K but that, on the other hand W_λ(4630.54 Å) > W_λ(5666.63 Å) for higher effective temperatures. The measured equivalent widths for all the target stars, listed in Table 2, indicates, however, that the measured W_λ(4630.54 Å) is always larger than W_λ(5666.63 Å) for the temperature range of the stars we are considering. Therefore, unless the equivalent widths are being improperly measured because of blends or for any other reason, the NLTE calculations predict the reverse trend of what we obtain from the observations for T_{eff} less than roughly 27,000 K. This could indicate that the NLTE abundances derived for the lines belonging to the triplet $3s\,^3P^o$–$3p\,^3D$ are incorrect. The inclusion of N II lines belonging to other multiplets would be helpful in determining the reliability of the NLTE calculations. This step would demand observa-

TABLE 9

ADDITIONAL NLTE N II ABUNDANCES FOR HD 35299

N II Line (Å)	W_λ	$\xi = 0.0$	$\xi = 5.0$	$\xi = 10.0$
4779.7	19	8.11	8.06	8.04
4781.2	7	8.04	8.04	8.04
4788.13	21	7.99	7.92	7.89

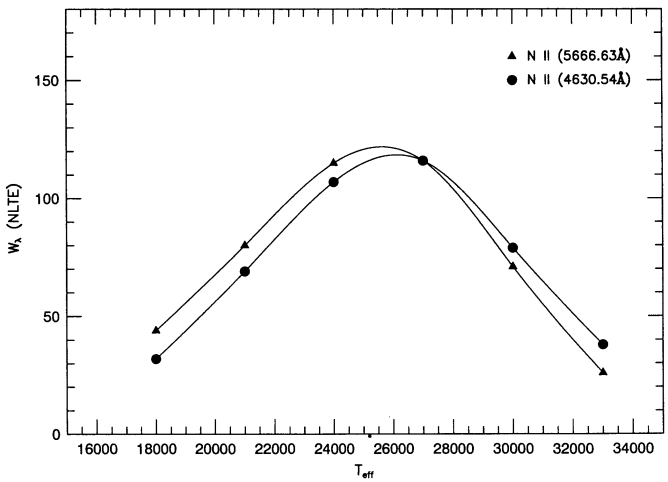

FIG. 16.—Change in the NLTE equivalent width of N II $\lambda\lambda$4630.54 (*filled circles*) and 5666.63 (*filled triangles*) as a function of the star's effective temperatures.

tions at different wavelengths. In the present paper we will consider the NLTE N II abundances as derived from the $3s\,^3P^o$–$3p\,^3P$ lines only.

The mean NLTE nitrogen abundances derived for the stars, and the standard errors of the mean, are listed in Table 7. These NLTE abundances were derived for microturbulences estimated from the O II, N II, and Si III lines. As shown in Figure 15, the NLTE N abundances decline with increasing $T_{\rm eff}$. This decline is quite similar to that obtained for carbon. (The very N-rich star HD 37042 is not plotted in Fig. 15 because its $T_{\rm eff}$ places it outside the grid of available NLTE calculations.)

In § 3.5.2 we discuss a possible origin for the $T_{\rm eff}$ dependence.

Oxygen.—The NLTE abundances are based on Paper I but have been recomputed for the new values of microturbulence. The NLTE oxygen abundances for the stars are listed in Table 7. HD 37023 required a slight extrapolation of the available grid of NLTE predictions. The mean NLTE oxygen abundances as a function of $T_{\rm eff}$ are presented in Figure 15. Inspection of the figure shows no significant trend of the abundances with $T_{\rm eff}$.

Silicon.—In order to derive NLTE abundances for our sample of Si II and Si III lines, we have used the equivalent width grid calculated by Becker & Butler (1990b), as supplemented by additional grid points kindly calculated by S. Becker. The model atom employed in the NLTE calculations included Si II, Si III, and Si IV, as described by Becker & Butler (1990a).

The differences between the LTE abundances of the Si III and Si II lines are reduced when NLTE calculations are considered. This will be discussed in § 3.5.2.

In Figure 15 we plot the derived NLTE Si abundances as a function of effective temperature, and, as for oxygen, no significant trend of the abundances with $T_{\rm eff}$ is found. As mentioned before, the mean Si abundances are represented by mean Si III abundances.

3.5.2. *NLTE and Model Atmospheres*

The available NLTE calculations are based on Gold's models, but the LTE calculations use Kurucz's more heavily blanketed models. We decided to make a preliminary assessment of the NLTE abundances that would result from use of Kurucz's models. It appears that this use most likely removes the $T_{\rm eff}$-dependent trends of the NLTE carbon and nitrogen abundances.

LTE abundances resulting from Kurucz and Gold models were readily estimated. Because of the differences in the temperature structure of the models, the LTE equivalent width of a given line reaches a maximum at a lower $T_{\rm eff}$ for the Kurucz models than for the Gold models. This is illustrated in Figure 14, where we plot the behavior of the equivalent width of the 4630 Å N II line with effective temperature. Differences in the derived abundances follow from this behavior. Abundance differences Δ = log ϵ(Gold) − log ϵ(Kurucz) are listed in Table 10 for models in the range $T_{\rm eff}$ = 18,000–30,000 K with log g = 4.0 (The Gold models were kindly provided by S. Becker 1993, private communication). These differences for the cooler stars exceed the uncertainties expected from the abundance analysis.

The demonstration that the selection of the family of models affects significantly the LTE abundances suggests that the selection will also be important for the derivation of the NLTE abundances. Since Kurucz's models, being more thoroughly line-blanketed, are probably more realistic, it is of interest to estimate NLTE abundances provided by his models. One possible way to make these estimates is to assume that NLTE effects are effectively identical for two families of models: i.e.,

$$\epsilon(\text{Kurucz})^{\rm NLTE} = \epsilon(\text{Gold})^{\rm NLTE} + [\epsilon(\text{Kurucz})^{\rm LTE} - \epsilon(\text{Gold})^{\rm LTE}] .$$

Then, Table 10 provides the necessary corrections with which one can estimate ϵ(Kurucz)$^{\rm NLTE}$. These estimates for C, N, O, and Si are shown in Figure 17.

Inspection of Figure 17 shows that these (approximate) NLTE abundances of carbon and nitrogen are independent of $T_{\rm eff}$, unlike the original NLTE abundances (Fig. 15). We supose that the $T_{\rm eff}$ independent results are more likely to be correct. In particular, we cannot identify an external reason why the carbon and nitrogen abundances should both decline with increasing $T_{\rm eff}$, as in Figure 15.

The NLTE abundances inferred for Kurucz's models for oxygen and silicon show higher abundances for the hottest ($T_{\rm eff}$ > 28,000 K) stars. As we discuss in § 4, we consider these trends to reflect the fact that the hottest stars, primarily from subgroup Id, are enriched in nucleosynthetic products of Type II supernovae.

An approximate measure of the effect of departures from LTE on the abundances is provided by Figure 17 and the LTE abundances in Table 6. The mean differences log ϵ(Kurucz)$^{\rm LTE}$ − log ϵ(Kurucz)$^{\rm NLTE}$ are 0.02, 0.13, 0.22, and 0.31 for C, N, O, and Si, respectively.

As previously discussed, the LTE Si II lines give significantly

TABLE 10

ABUNDANCE DIFFERENCES

$T_{\rm eff}$ (K)	Δ(O II)	Δ(N II)	Δ(C II)	Δ(Si II)	Δ(Si III)
18,000	0.24	0.20	0.18	−0.08	0.22
20,000	0.27	0.22	0.16	−0.14	0.26
24,000	0.20	0.08	−0.02	−0.25	0.17
27,000	0.02	−0.10	−0.09	−0.42	−0.07
30,000	0.00	−0.01	0.01	−0.16	−0.10

NOTE.—Δ = difference between the LTE abundances calculated with Gold's and Kurucz's models for log g = 4.0.

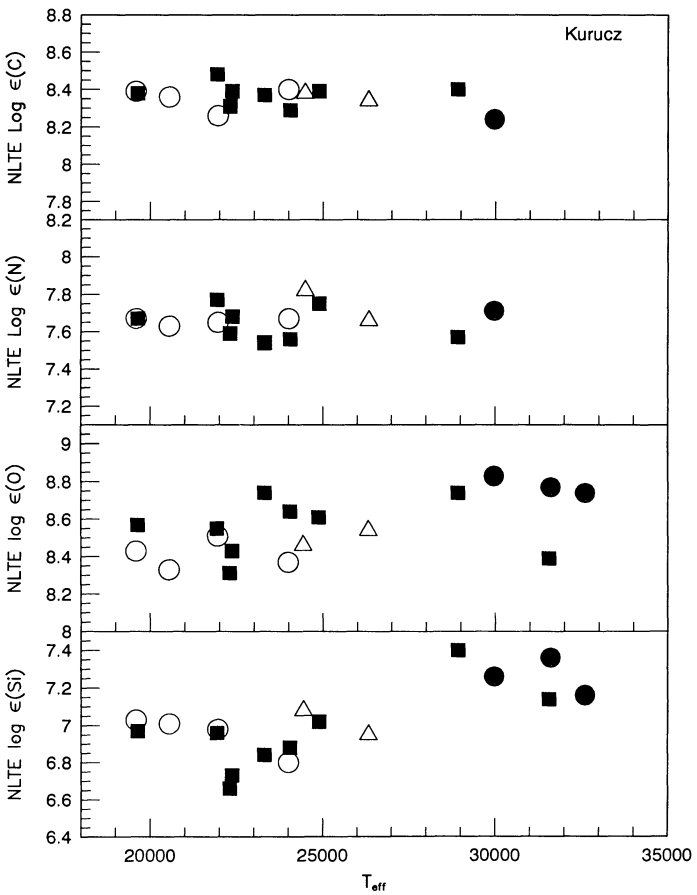

FIG. 17.—Mean NLTE carbon, nitrogen, oxygen, and silicon abundances as a function of the stars' effective temperatures. The calculations were done by means of Kurucz's model atmospheres. The symbols used to distinguish the four subgroups are described in Fig. 7.

lower abundances than the Si III lines. The mean differences between the LTE Si III and Si II abundances for the studied stars is about +0.4 dex. This difference becomes roughly +0.1 dex when the NLTE calculations based on Gold's models are considered, and becomes even smaller when we consider the estimated NLTE abundances based on Kurucz's models.

Our suggestion that the presently available NLTE calculations are the origin of the $T_{\rm eff}$-dependent abundances for carbon and nitrogen will be tested when the calculations are redone with Kurucz's models. Our assumption that the NLTE effects are not greatly dependent on the model family has been tested with calculations (S. Becker 1993, private communication) of NLTE equivalent widths for O II lines based on selected Kurucz and Gold model atmospheres. The differences in the calculated NLTE equivalent widths of the O II lines yielded abundance differences Δ(NLTE) which are similar to the abundance differences Δ(LTE) presented in Table 10. The calculated mean of the abundance differences Δ(LTE) − Δ(NLTE) is 0.09 ± 0.04 dex. Therefore, our assumption seems to be fairly well supported.

3.6. *Abundance Uncertainties*

Before turning to the next section, where we discuss our derived abundances in terms of self-enrichment of the Orion association, we assess the accuracy of our derived abundances.

The internal errors of the abundances for each program star are listed in Tables 6 and 7 for the LTE and NLTE abundances, respectively. These errors represent the line-to-line scatter of the abundances, which is mainly due to uncertainties in the measured equivalent widths, errors in the atomic data used, and errors due to uncertainties in the adopted microturbulence velocity. The scatter in the LTE abundances may, in part, also be due to the neglect of NLTE effects, as the NLTE corrections can be of different magnitudes for different lines. Inspection of Tables 6 and 7 shows that the standard error for the derived mean abundances is typically about 0.05–0.10 dex. Such a standard error is compatible with the expected error from combining the uncertainties in the measured equivalent widths (10%–15%) and in the *gf*-values of the lines (10%–15%), and the errors due to uncertainties in the microturbulence ($\sim \pm 1.5$ km s^{-1}).

The observed C II, N II, O II, and Si III span quite a small range in excitation potential. Therefore, the line-to-line scatter of these abundances should not be changed significantly when $T_{\rm eff}$ is adjusted within its expected errors. On the other hand, the Fe III lines span a wider range in excitation potential, and, hence, the line-to-line scatter in the iron abundances, besides reflecting the sources of internal errors discussed above, may also reflect errors due to the fact that we are averaging lines spanning a significantly larger range in excitation potentials.

Another source of errors in the derived abundances are those due to the uncertainties in the stellar parameters $T_{\rm eff}$, g, and microturbulence. As discussed above, we estimate that the measurement and systematic errors amount to about 3% in $T_{\rm eff}$ and about 0.1 dex in log g. The uncertainties in the derived microturbulent velocities are estimated to be about ±1.5 km s^{-1}. As in Paper I, we selected representative stars with effective temperatures covering the $T_{\rm eff}$ extremes of our sample and recalculated the elemental abundances with slightly different model atmospheres. The changes to the carbon, nitrogen, silicon, and iron abundances resulting from increases of 3% for $T_{\rm eff}$, 0.1 dex for log g, and 1.5 km s^{-1} for the microturbulence are summarized in Table 11. We note that when $T_{\rm eff}$ was changed log g was kept constant and vice versa.

As an additional check on the measurement errors, we rederived the abundances adopting the effective temperatures derived with NSW codes (see § 3.2). These derived C, N, O, and Si LTE abundances are typically within 0.05 dex of the abundances in Table 6, and the dispersion of the abundances is essentially unaltered.

As we discussed in presenting the NLTE abundances of C II and N II, the tendency for the abundances to decline with increasing $T_{\rm eff}$ may be due to the use of inadequately line-blanketed models in the computation of the NLTE effects. Other uncertainties affecting the NLTE abundances are almost impossible to evaluate: e.g., the size of the model atom. But since the predicted departures from LTE are small for the C II, N II, and O II lines, we suppose that the NLTE abundances are subject to very small additional uncertainties.

Due to the importance of attempting to separate abundance changes due to errors in $T_{\rm eff}$, log g, and ξ from intrinsic abundance spreads in the Orion stars, we performed a simulation of abundance differences induced by random errors in the stellar parameters and compared these with the real abundance distributions. We assume that our estimated uncertainties of 3% in $T_{\rm eff}$, 0.1 dex in log g, and 1.5 km s^{-1} in ξ represent approximately 1 σ values of Gaussian-distributed random errors. We use these values to generate random Gaussian-distributed errors in $T_{\rm eff}$, log g, and ξ for the representative model atmo-

TABLE 11

ABUNDANCE UNCERTAINTIES

Element	δ	HD 35039 (20,550/3.74)[a]	HD 36591 (26,330/4.21)[a]	HD 36960 (28,920/4.33)[a]	HD 37023 (32,600/4.70)[a]
C	$\delta(T_{\rm eff})$	−0.04	+0.02	+0.06	...
C	$\delta(\log g)$	+0.03	−0.01	−0.02	...
C	$\delta(\xi)$	−0.01	0.00	−0.01	...
N	$\delta(T_{\rm eff})$	−0.10	+0.04	+0.10	...
N	$\delta(\log g)$	+0.05	+0.01	−0.01	...
N	$\delta(\xi)$	−0.03	−0.02	−0.01	...
O	$\delta(T_{\rm eff})$	−0.15	−0.08	0.00	+0.12
O	$\delta(\log g)$	+0.06	+0.03	0.00	−0.02
O	$\delta(\xi)$	−0.05	−0.09	−0.07	−0.07
Si	$\delta(T_{\rm eff})$	−0.12	+0.03	+0.09	+0.21
Si	$\delta(\log g)$	+0.07	+0.02	−0.02	−0.02
Si	$\delta(\xi)$	−0.10	−0.10	−0.10	−0.05
Fe	$\delta(T_{\rm eff})$	−0.06	+0.04	+0.09	...
Fe	$\delta(\log g)$	+0.05	+0.01	−0.01	...
Fe	$\delta(\xi)$	−0.01	−0.01	−0.01	...

[a] $T_{\rm eff}$ (K) and $\log g$; see Table 1.

spheres for our sample and use the randomly perturbed stellar parameters to derive new abundances (using Table 11), assuming we start with zero intrinsic abundance dispersions in C, N, O, and Si. The results of this Monte Carlo simulation are illustrated in Figure 18, where we plot frequency histograms of the abundances for the four elements from the observed stars (*left-hand panels*) and from the simulation (*right-hand panels*). In order to realistically compare a simulation to the real results, we perform a simulation for the same number of points as observed stars (18), with 6 simulated points taken from the cool model, 6 from the medium and 3 each from the two hotter models for C and N, while for O and Si we used 6 points each from the cooler models and 3 points each from the two hottest models. This difference is due to the fact that there were no measured equivalent widths for the hottest star in our sample. We bin the data and simulated data by 0.05 dex, which is close to the expected best results and also coincides closely with the accuracies of the *gf*-values. On top of the observed and simulated histograms we plot Gaussians defined by our random-number generators: these functions represent the limit of the distributions which would result from running the simulation an infinite number of times, and we normalize the areas to be equal to the areas of the finite histograms. It is clear that the finite simulations closely approximate the expected limiting distributions, and a χ^2 comparison shows excellent agreement. For example, a comparison of the respective C, N, O, and Si simulations with the limiting Gaussian function yields χ^2 values of 4.3 ($n = 5$), 2.7 ($n = 6$), 4.5 ($n = 8$), and 3.8 ($n = 7$). All of these values satisfy the criterion of a good fit: $\chi^2 \leq n$ (where n is the number of binned comparison points). Concerning the observed abundance distributions, both C and N are also described very well by the simulation, and this good agreement is also shown by a χ^2 test: $\chi^2 = 6.4$ ($n = 5$) for carbon, $\chi^2 = 2.0$ ($n = 6$) for nitrogen. Oxygen and silicon, on the other hand, are not represented at all by the simulated distributions, and a χ^2 comparison results in enormous values for χ^2: $\chi^2 = 46$ ($n = 9$) for oxygen and $\chi^2 = 29$ ($n = 9$) for silicon. Either there are real abundance differences inherent in the Orion stars in our sample, or we have grossly underestimated our errors (although C and N fit the estimates very well). We have adopted conservative estimates of the errors, and we do not expect these to be significantly bigger. The Monte Carlo simulations also provide estimates of the correlations between the elemental abundances that result from uncertainties in the atmospheric parameters.

4. DISCUSSION

A massive star belonging to an OB association may on explosion as a supernova contaminate gas in the neighboring molecular clouds with freshly synthesized elements. Then a later generation of stars formed in the clouds will exhibit this "self-enrichment."

In Paper I we showed that the oxygen abundances of 18 main-sequence stars from the four subgroups of the Orion association suggested that a degree of self-enrichment has occurred. The evidence was as follows:

1. The stars in the youngest subgroup (Id) and some of the stars in subgroup Ic are enriched in oxygen by about 40% relative to the stars belonging to the two oldest subgroups (Ia and Ib).
2. The most O-rich stars are close together in space, well separated from the stars of lower oxygen abundance.

In this section we examine the idea of self-enrichment more closely, using the new abundances of C, N, Si, and Fe with the (redetermined) O abundances. We also comment briefly on the stellar and interstellar (the H II region) composition, and the N-rich star HD 37042.

4.1. *Signatures of Self-Enrichment*

The most likely polluters of a molecular cloud near an OB association will be the most massive (i.e., shortest-lived) stars. Calculations of explosive nucleosynthesis by these stars show that their ejecta are substantially overabundant (relative to the solar composition) in oxygen. Other major products are Ne, Mg, Si, and S. For example, Thielemann, Nomoto, & Hashimoto (1993) predict that a 25 $M_\odot$ star will eject 3.0 $M_\odot$ of O, 0.15 $M_\odot$ of C, and 0.12 $M_\odot$ of Si, or the relative number of atoms in the ejecta is O:C:Si = 1:0.07:0.02, where the solar mix corresponds to the ratios 1:0.50:0.05. This calculation suggests that an O enrichment, as found in Paper I, should be accompanied by a similar Si enrichment, but enrichment of C

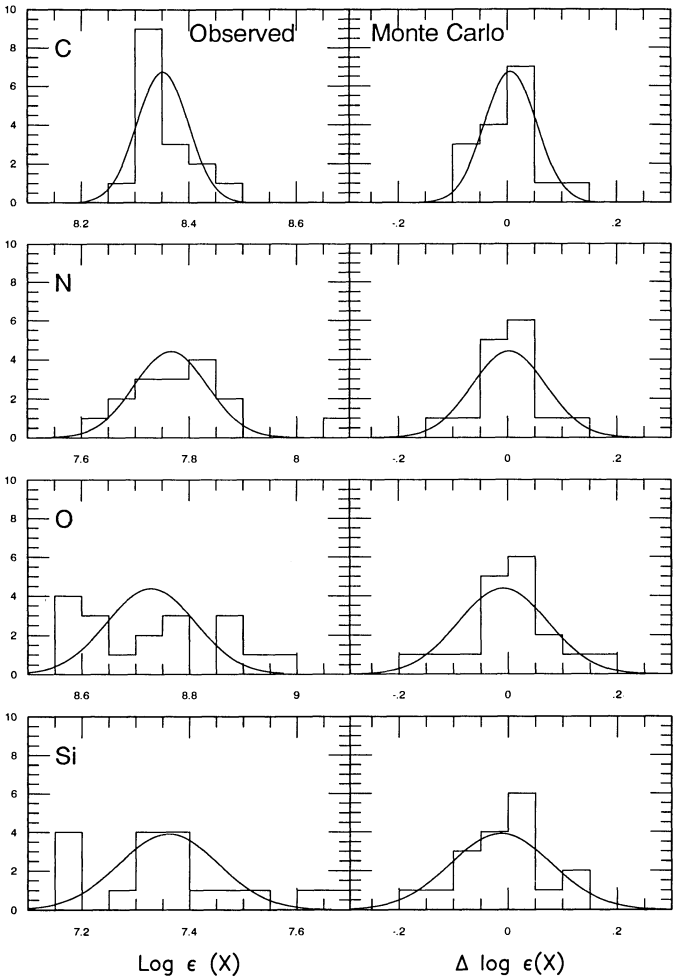

FIG. 18.—Frequency abundance histograms both for observed stars (*left-hand panels*) and from a Monte Carlo simulation (*right-hand panels*) which includes random errors in $T_{\rm eff}$, log g, and ξ and starting with a uniform abundance for each element. The observed abundances correspond to the LTE-derived abundances. The superposed Gaussians represent the limiting distributions expected from our error simulations. Each finite Monte Carlo simulation (which contains the same number of points as the corresponding observed histogram) is fitted very well by the limiting Gaussian. For the observed histograms, both C and N and are also fitted very well by the limiting expected error distribution, while O and Si exhibit more scatter than can be accounted for by our error estimates.

is quite unlikely. Therefore, we begin the discussion by examining the variation of the abundances relative to that of oxygen. The LTE abundances of C, N, and Fe versus O, and Si versus O, are shown respectively in Figure 19 and in the top panel of Figure 20, where we prefer the LTE to the NLTE abundances because the latter as given in Table 10 seem subject to a relatively large uncertainty arising from the use of lightly blanketed models. The NLTE abundances as approximately corrected for the differences between the Gold and Kurucz models support our conclusions drawn from the LTE abundances.

The C abundance is obviously independent of the O abundance: the total spread in the former is 0.21 dex, against 0.40 dex for the latter. This result is in accord with the simple prediction just outlined for self-enrichment by supernovae. The Monte Carlo simulations predict the spreads, but the measured oxygen abundances are not distributed as predicted by the simulations (Fig. 18).

Similarly, the nitrogen abundances show no trend with the O abundances. The spread for nitrogen is only slightly larger than for carbon: 0.25 dex for N, excluding the N-rich star HD 37042. Only a small part of the spread of 0.25 dex can be due to contamination of a stellar atmosphere by CN-cycled material from within the star (or in a supernova's ejecta); the observed spread is essentially equal to that predicted by the Monte Carlo simulations. Although the CN cycle necessarily produces a N enrichment by the conversion of C to N with the preservation of the total number of C and N nuclei, a N enrichment at the low levels seen here (HD 37042 is an exception) does not require a measurable loss of carbon: for example, a reduction of the C abundance by only 0.05 dex, from log ϵ(C) = 8.35 to log ϵ(C) = 8.30, raises a N abundance of log ϵ(N) = 7.75 to log ϵ(N) = 7.91. Further discussion of the N abundances is given in § 4.2.

The Si abundances show a larger spread (0.50 dex); the standard deviation from Table 6 is 0.14 dex (18 stars) for Si, 0.13 dex (18 stars) for O, and only 0.06 dex for C (16 stars). As discussed in § 3.6, the abundance spreads for C and N are compatible with what is expected from random errors in the abundances, but in order to explain the spread in O and Si errors we would need to increase the errors and to identify a systematic error that gives rise to a non-Gaussian distribution of abundances (Fig. 18). The Si and O abundances appear to be correlated. As shown in Figure 20, the random errors can produce a spurious correlation of the Si abundance with the O

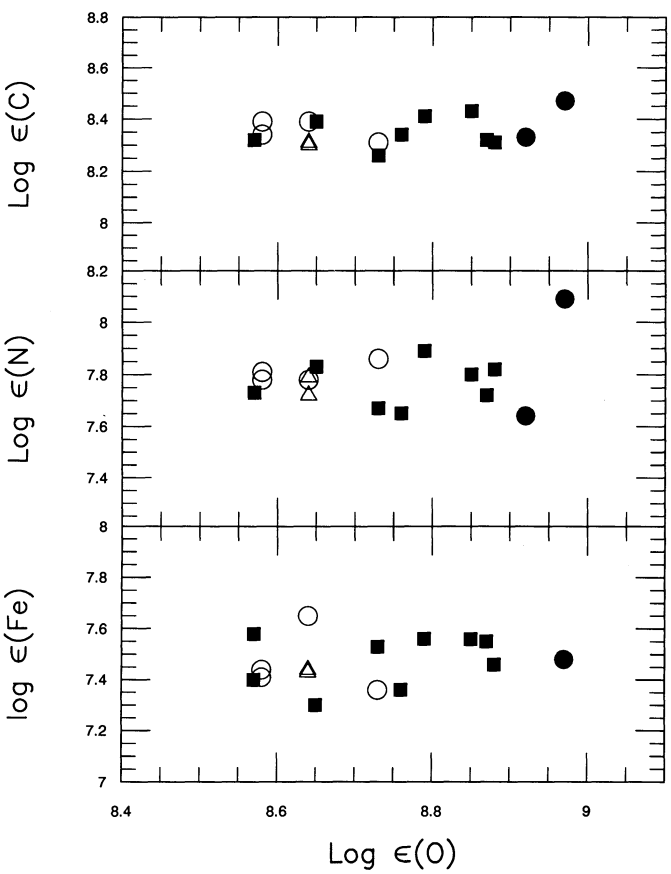

FIG. 19.—LTE carbon, nitrogen, and iron abundances as a function of oxygen abundances. The symbols used to distinguish the four subgroups are described in Fig. 7.

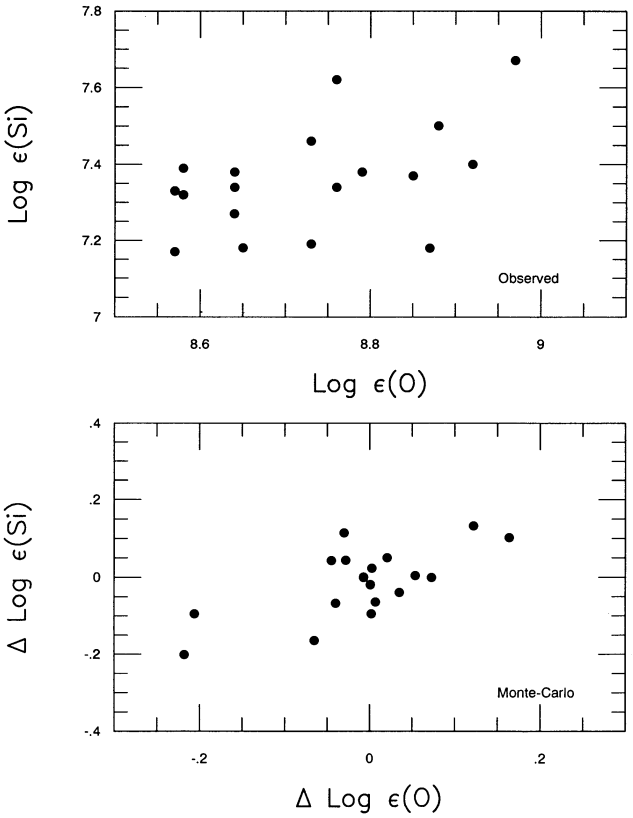

FIG. 20.—LTE observed silicon abundances as a function of oxygen abundances (*top panel*) and Si abundances as a function of oxygen abundances from a Monte Carlo simulation (*bottom panel*).

abundance: in Figure 20 we show the observed Si and O abundances in the top panel and the simulated abundances in the bottom panel. Clearly, the observed Si and O abundances are more evenly dispersed over their respective total ranges than the simulated abundances from the Monte Carlo test. We suppose that the larger dispersion may reflect real abundance differences between the stars. In support of the supposition we note that the O- and Si-enriched stars are collocated. A suspicion that therefore the effective temperatures of these stars are systematically in error owing to a consistent error in the estimated reddenings may be allayed by the fact that the enriched stars have a considerable range in the assigned reddenings.

The Fe abundances exhibit a scatter slightly less than that shown by the O abundances: the total spread and standard deviation are 0.35 dex and 0.10 dex, respectively, for Fe, and 0.40 dex and 0.13 dex for O. In contrast to Si, Fe does not appear to be correlated with the O abundances.

This initial discussion shows that O and Si, both principal products of massive stars (Type II supernovae or SN II), are likely enriched in certain stars in a common region of the association; we showed in Paper I that the O-enriched stars from the youngest (Ic and Id) subgroups of the association are at a common distance from the Sun and clustered around a point on the sky (the Trapezium). The Si-enriched stars are found in the same parts of the association. Carbon, a minor product of Type II supernovae, is not enriched in these stars.

Next, we investigate whether the ratio of the O to Si yields derived from our abundances is consistent with predictions of yields for SN II. We adopt a simple model for the mixing of SN ejecta with ambient gas. We assume that the ejecta do not contain hydrogen. This seems a reasonable assumption because the H-rich gas shed before and during the SN explosion will contain roughly normal abundances of O and Si (the C and N abundances may be changed by CN-cycling), and hence this gas counts as ambient gas. In this model the total mass [M(T)] of the mixture will be

$$M(\mathrm{T}) = M(\mathrm{A}) + M(\mathrm{SN}) ,$$

where M(A) and M(SN) are respectively the mass of the ambient cloud and the mass ejected by the supernova. The O content of the total (ambient plus SN) mixture is therefore

$$M(\mathrm{T}, \mathrm{O}) = M(\mathrm{A}, \mathrm{O}) + M(\mathrm{SN}, \mathrm{O}) ,$$

or

$$Z(\mathrm{T}, \mathrm{O})M(\mathrm{T}) = Z(\mathrm{A}, \mathrm{O})M(\mathrm{A}) + Z(\mathrm{SN}, \mathrm{O})M(\mathrm{SN}) ,$$

where Z(O) is the mass fraction of oxygen. If we assume that the total mass ejected by the supernova is negligible compared with the mass of the ambient cloud, we have

$$Z(\mathrm{T}, \mathrm{O}) = Z(\mathrm{A}, \mathrm{O})\left[1 + \frac{Z(\mathrm{SN}, \mathrm{O})}{Z(\mathrm{A}, \mathrm{O})}\frac{M(\mathrm{SN})}{M(\mathrm{A})}\right] ,$$

and the increase of the O abundance between the most O-poor (ambient gas) and the most O-rich (total gas) stars is proportional to the factor Z(SN, O) and the ratio M(SN)/M(A). Comparison of the increases of the O and Si abundances then gives the ratio Z(SN, O)/Z(SN, Si).

Examination of the top panel of Figure 20 shows that the O/Si abundance ratio is approximately constant and close to the solar ratio (O/Si = $10^{1.3}$). The slope of the least-squares fit corresponds to Z(SN, O)/Z(SN, Si) $\simeq 25 \pm 15$; the uncertainty was estimated from the slope that could represent the minimum oxygen and silicon and the maximum silicon and oxygen abundances in the sample. The slope reflects in part the correlated errors of the O and Si abundances. The NLTE abundances (from Gold's models) indicate a slightly higher ratio. Solar abundances correspond to Z(O)/Z(Si) = 13.

In a simple picture of self-enrichment in Orion, the inferred Z(O)/Z(Si) represents the average yield of the supernova ejecta mixed into the interstellar gas of the association from supernovae of differing progenitor masses and differing Z(O)/Z(Si). Inspection of the models of Thielemann et al. (1993) shows that such a ratio Z(O)/Z(Si) would be typical of the most massive stars: for example, their 25 $M_\odot$ model gives a ratio of the yields of 26, while this ratio drops to 16 for a 20 $M_\odot$ progenitor and to 6 for a 15 $M_\odot$ model.

Given the age of the Orion association of about 10^7 yr, one would expect that only those stars more massive than roughly 16 $M_\odot$ would have had time to complete their evolution. Reeves (1978) estimated that 10–20 supernova explosions occurred in the Orion association. Assuming that 17 stars exploded as supernovae, we approximate the mass distribution for the stars as follows (based on Miller & Scalo's 1979 mass function): seven stars of 15 $M_\odot$, four stars of 20 $M_\odot$, three stars of 25 $M_\odot$, two stars of 35 $M_\odot$ and one star of 50 $M_\odot$. By assuming the elemental yields from the stars of different masses as calculated by Woosley & Weaver (1986), we estimate Z(O)/Z(Si) to be about 5. In these calculations we used the yields predicted by Woosley & Weaver (1986) instead of the more recent calculations of Thielemann et al. (1993) because only Woosley & Weaver published the yields for the most massive

stars. The predicted yields of oxygen from the two calculations are in quite good agreement for stars of 15, 20, and 25 $M_\odot$ stars. The yields of silicon, however, are a factor of 3 higher in Woosley & Weaver's calculations. If one assumes that the Si yields calculated by Thielemann et al. (1993) are also a factor of 3 smaller than Woosley & Weaver's (1986) for the most massive stars, we predict $Z(\mathrm{O})/Z(\mathrm{Si}) \simeq 15$. This ratio is more compatible with the inferred ratio of $Z(\mathrm{O})/Z(\mathrm{Si}) \simeq 25 \pm 15$.

An additional constraint on this scenario is provided by our carbon abundances. Recall from Figure 19 that no detectable increase in the carbon abundance is found as the oxygen abundance increases by almost a factor of 2. These observations can set limits on the ratios of the yields of carbon to oxygen in the presumed supernova ejecta. The limit that we can set (see § 3.4) on a carbon abundance increase is less than 0.05 dex. If so, as the oxygen abundances increase from $\log \epsilon(\mathrm{O}) = 8.55$ to $\log \epsilon(\mathrm{O}) = 8.85$, then an increase in the carbon abundance no larger than 0.05 dex implies $Z(\mathrm{C})/Z(\mathrm{O}) < 0.05$. The 25 $M_\odot$ model of Thielemann et al. (1993), predict $Z(\mathrm{C})/Z(\mathrm{O}) = 0.05$ which is consistent with our estimated upper limits for the observed C abundances.

This simple picture of supernova self-enrichment across the Orion association over the past 10^7 yr agrees with the pattern of the derived abundances of O, Si, and C. Nitrogen fits the picture too, because it is not expected to be produced in large quantities in massive supernovae. But interpretation of N abundances needs to recognize that they may be altered as CN-cycled material is mixed to the surface of the star (see § 4.2).

We have not included Fe in our previous discussions because the predicted yields are not large and are quite uncertain because of uncertainties in the mass cut between ejecta and the core of the neutron star. However, as a comparison, let us adopt the the predicted yields for O and Fe from the 20 $M_\odot$ model for SN 1987A (Hashimoto, Nomoto, & Shigeyama 1989), which is constrained by the observed light curve of this supernova. If we assume an enhancement in the oxygen abundance from 8.55 to 8.85, we would obtain an enhancement in the Fe abundance of about 0.06 dex when mixing with a material with solar composition. From Figure 19 we see, as predicted, no significant enhancement of the oxygen with Fe abundances.

Our discussion has focused on the effect of SN ejecta in changing the relative abundances of O, Si, and C. It is also necessary to show that a sufficient amount of mass is ejected and entrained by the local dense molecular cloud to alter the cloud's chemical composition. Our discussion of this question in Paper I suggested that mixing of ejecta and ambient gas was possible.

4.2. *Nitrogen and* CN-*cycled Material*

With the exception of HD 37042, the LTE N abundances of our sample are spread over 0.25 dex. Carbon abundances show a slightly smaller spread of 0.21 dex. As shown in § 3.6, these spreads are approximately consistent with those expected from the measurement errors applied to stars all of the same composition.

There is a hint that C and N abundances are positvely correlated, but this may reflect the similar sensitivities of these elemental abundances to T_{eff} and g errors (see Table 11). The C/N ratios are equal to within $\pm 25\%$ for all stars except the N-rich star HD 37042. In short, the sample apart from HD 37042 offers no evidence that the atmospheres have been mixed with CN-cycled material from the interiors (or elsewhere). This result is not inconsistent with Gies & Lambert's (1992) survey of B stars of similar effective temperatures, which showed just a few stars to exhibit N-enrichment. HD 37042 is presumably contaminated with CN-cycled material; we note, however, that it is also the most C-rich star of the sample but the requirement that the sum of C and N be conserved is met within the anticipated uncertainties.

The NLTE abundances similarly show a nearly constant C/N ratio close to the solar value. (The NLTE N abundances could not be computed for HD 37042.) In contrast to the LTE abundances, there is a clear correlation between C and N abundances for the NLTE abundances calculated from Gold's models. Both are spread over about 0.35 dex. This spread is not due to admixtures of CN-cycled material because the correlation is a positive one and not negative. The correlation is a reflection of the apparent systematic T_{eff}-dependent error of NLTE abundances that results from the use of mildly blanketed model atmospheres.

4.3. *Composition of Gas and Stars in Orion*

The Orion Nebula, specifically M42, has been observed spectroscopically many times in order to derive fundamental characteristics such as gas density, temperature, and chemical composition. Studies of the nebula's chemical composition have, in general, concluded that its carbon, nitrogen, and oxygen abundances are lower than the solar values. To some this proves a puzzling result; simple models of galactic chemical evolution predict the Sun, an older object, to be less enriched than a young nebula such as M42 in products of stellar nucleosynthesis like carbon, nitrogen, and oxygen. Indeed, Reeves (1978) suggested that there could arise a spread of compositions in an OB association, and the Sun was born from a self-enriched portion of an association. Our study of the chemical compositions of stars in the Orion association provides a check on the nebular abundances.

For the comparison of stars and gas, we elect to stress the use of the mean LTE abundances for the 12 stars from the two youngest subgroups, Ic and Id. The LTE abundances are perhaps slightly more reliable than the NLTE abundances presently available, but in Table 12 we give both the LTE and the NLTE abundances as estimated from Kurucz model atmospheres. Subgroups Ic and Id are more representative of M42 than the older subgroups Ia and Ib, which are set apart in the sky from the Orion Nebula. Nebular abundances are given in Table 12 from the several studies reported since 1991; Baldwin et al. (1991), Rubin et al. (1991) with Rubin, Dufour, & Walter (1993) for the C abundance, Osterbrock, Tran, & Veilleux (1992), and Peimbert, Storey, & Torres-Peimbert (1993), as well as the unweighted average of the abundances in these nebular studies. Walter, Dufour, & Hester's (1992) analysis is not included because their preferred abundances are dependent on the adopted size of the temperature fluctuations in the H II region, but the authors provide essentially no independent evidence for the adopted fluctuations; an argument based on the ionizing flux from the stars uses incompletely blanketed model atmospheres. We also refer the abundances of the Orion stars and gas to the solar composition, which for C, N, and O we take from Grevesse & Noels (1993), who recalculate these abundances taking into account the effect of the recent downward revision of the solar Fe abundance on the gas and electron pressures in the solar model atmosphere. Results are collected in Table 12.

TABLE 12

C, N, AND O ABUNDANCES OF THE SUN, THE ORION STARS, AND THE ORION NEBULA

ELEMENT	B STARS[a] (CL93)	NEBULA[b] B91	R91	O92	R93	P93	AV	SUN[c] (GN93)
C	8.36 ± 0.06/8.36 ± 0.07	8.33	8.53	...	8.45	8.53	8.46	8.55 ± 0.05
N	7.84 ± 0.13/7.65 ± 0.09	7.94	7.83	7.57	...	7.87	7.80	7.97 ± 0.07
O	8.78 ± 0.13/8.61 ± 0.17	9.58	8.60	8.49	...	8.76	8.61	8.87 ± 0.07

[a] CL93 = Cunha & Lambert (this paper); the first set of values indicate the LTE (Kurucz) abundance averages, and the second one indicates the estimated NLTE (Kurucz) abundance averages.

[b] B91 = Baldwin et al. 1991; R91 = Rubin et al. 1991; O92 = Osterbrock, Tran, & Veilleux 1992; R93 = Rubin, Dufour, & Walter 1993; P93 = Peimbert, Storey, & Torres-Peimbert 1993; AV = average of nebular abundances.

[c] GN 93 = Grevesse & Noels 1993.

Inspection of Table 12 shows that the Orion stars are, relative to the Sun, deficient in C, N, and O by 0.09–0.19 dex if the stellar LTE abudances are selected. Differences are somewhat larger for the NLTE stellar abundances. These differences exceed those expected from the measurement uncertainties. With respect to the chemical evolution of the Galaxy, the subsolar abundances of the Orion stars is a problem only for the simplest theories of this chemical evolution. The result is not a surprise when Orion stars are measured against others in the solar neighborhood. Young stars and open clusters show a spread in metallicity (and abundances of C, N, and O too) that encompasses the solar and Orion values (Luck & Lambert 1985: Nissen 1988; Boesgaard 1989; Edvardsson et al. 1993). Judged against its neighbors, Orion is not anomalous. (In Paper I we summarized the viewpoint that the Orion association has been captured from the Magellanic stream of metal-poor objects.)

Are the stellar and nebular abundances concordant? Answering this question is difficult because essentially no error estimates are provided for the nebular abundances, but inspection shows that they are likely to be quite concordant. For example, Peimbert et al.'s (1993) N and O abundances are within 0.03 dex and −0.02 dex, respectively, of the stellar LTE abundances. The comparable difference for C is 0.19 dex, but most probably a more reliable result is provided by Rubin et al. (1993), whose abundance is only 0.09 dex larger than the stellar LTE value. These very small differences must be judged against the larger differences arising in some of the nebular analyses from an assumption about the magnitude of the temperature fluctuations across the H II region. For example, Peimbert et al. set the parameter describing these fluctuations at $t^2 = 0.04$ on the basis of observations. The abundances in Table 12 are based on this choice, but if the fluctuations are presumed absent ($t^2 = 0$), the C, N, and O abundances are decreased by −0.01, 0.22, and 0.25 dex, respectively. One might imagine that systematic errors might be reduced by averaging the results of the several analyses in Table 12; a variety of observations and analytical techniques have been employed. The unweighted averages are 0.10, −0.04 and −0.17 dex larger than the LTE stellar abundances. Such a comparison does not recognize that the ionized gas may be depleted in some elements that are in the dust grains: Meyer (1985) estimates that 20% of the oxygen is locked in grains, i.e., the tabulated nebular abundances of O should be increased by 0.08 dex. In summary, we conclude that there is no compelling evidence for a difference between the composition of the stars and that of the gas in Orion but this region does have subsolar abundances of C, N, and O. (Silicon is definitely underabundant in the H II region, but this is due to incorporation of Si into the dust grains; see Rubin et al. 1993.)

5. CONCLUSIONS

We have presented abundances of C, N, Si, and Fe in 18 main-sequence B stars from across the Orion association; these abundances complement our earlier analysis of the oxygen abundances in these same stars (Paper I). We find that the C, N, and Fe abundances show no significant variations across the Orion subgroups, whereas the silicon abundances show a large scatter, which is similar to what was found for the oxygen abundance. The variations in the C and N abundances are in perfect agreement with what we expect from our estimates of the random errors inherent in our analysis. O and Si, on the other hand, exhibit larger abundance variations than can be accounted for by the identifiable errors, and, hence, either the errors have been incorrectly characterized for Si and O or the abundance variations are real. The most oxygen-rich and silicon-rich stars belong to the youngest subgroups in the association and reside in a common part of the association. The abundances are consistent with the picture sketched by Reeves (1978) in which massive stars exploded and polluted the Orion association before the oxygen-rich and silicon-rich stars formed. The pattern of oxygen and silicon enrichments and no detectable enrichment of carbon, nitrogen, and iron is consistent with the nucleosynthesis expected of Type II supernovae. The pattern, however, somewhat resembles that predicted from our Monte Carlo test, but we have argued that a real signature of chemical enrichment by Type II supernovae is probable.

Our C, N, and O abundances for the youngest subgroups (Ic and Id) of Orion agree with the averages from the Orion Nebula: all of these abundances are below solar by roughly 0.2 dex. These results strengthen the conclusion that the Orion association's abundances, in general, are below solar.

We are most especially indebted to Sylvia Becker for answering our many questions about the NLTE calculations and for providing the results of additional calculations made at our request. We thank Doug Gies, Ramiro de la Reza, Craig Wheeler, and John Scalo for several discussions; R. Napiwotski for the use of his computer code; Anil Pradhan and Sultana Nahar for providing Opacity Project *f*-values for some transitions; and especially Verne Smith for valuable and frequent advice. This research has been supported in part by the National Science Foundation (grant AST 91-15090) and the Robert A. Welch Foundation. K. C. acknowledges a fellowship from CNPq-Brasil.

REFERENCES

Abt, H. A. 1970, AJ, 75, 1095
Aller, L. H., & Jugaku, J. 1958, ApJ, 127, 125
Baldwin, J. A., Ferland, G. J., Martin, P. G., Corbin, M. R., Cota, S. A., Peterson, B. M., & Slettebak, A. 1991, ApJ, 374, 580
Balona, L. A. 1984, MNRAS, 211, 973
Becker, S. R., & Butler, K. 1988, A&AS, 76, 331
———. 1989, A&A, 209, 244
———. 1990a, A&A, 235, 326
———. 1990b, A&AS, 84, 95
Blaauw, A. 1991, in The Physics of Star Formation and Early Stellar Evolution, ed. C. J. Lada & N. D. Kylafis (Dordrecht: Kluwer), 125
Boesgaard, A. M. 1989, ApJ, 336, 798
Code, A. D., Davis, J., Bless, R. C., & Hanbury Brown, R. 1976, ApJ, 203, 417
Collins, G. W., II, 1970, ApJ, 159, 583
Collins, G. W., II, & Sonneborn, G. H. 1977, ApJS, 34, 41
Collins, G. W., II, Truax, R. J., & Cranmer, S. R. 1991, ApJS, 77, 541
Cunha, K., & Lambert, D. L. 1992, ApJ, 399, 586 (Paper I)
Eber, F., & Butler, K. 1988, A&A, 202, 153
Edvardsson, B., Andersen, J., Gustafsson, B., Lambert, D. L., Nissen, P. E., & Tomkin, J. 1993, A&A, 275, 101
Gies, D. R., & Lambert, D. L. 1992, ApJ, 387, 673 (GL)
Gold, M. 1984, Diplomarbeit, Ludwig Maximilian Universität
Goudis, C. 1982, The Orion Complex: A Case Study of Interstellar Matter (Dordrecht: Reidel)
Grevesse, N., & Noels, A. 1993, in Origin and Evolution of the Elements, ed. N. Prantzos, E. Vangioni-Flam, & M. Cassé (Cambridge: Cambridge Univ. Press), 15
Habets, G. M. H. J., & Heintze, J. R. W. 1981, A&AS, 46, 193
Hanbury Brown, R., Davis, J., & Allen, L. R. 1974, MNRAS, 167, 121
Hashimoto, M., Nomoto, K., & Shigeyama, T. 1989, A&A, 210, L5
Herrero, A. 1987, A&A, 171, 189
Kilian, J., Becker, S. R., Gehren, T., & Nissen, P. E. 1991a, A&A, 244, 419
Kilian, J., Montenbruck, O., & Nissen, P. E. 1991b, A&AS, 88, 101
Kilian, J., & Nissen, P. E. 1989, A&AS, 80, 255 (KN)
Kurucz, R. L. 1979, ApJS, 40, 1
Kurucz, R. L., & Peytremann, E. 1975, Smithsonian Astrophys. Obs. Spec. Rep. 362 (KP)
Lester, J. B., Gray, R. O., & Kurucz, R. L. 1986, ApJS, 61, 509 (LGK)
Luck, R. E., & Lambert, D. L. 1985, ApJ, 298, 782
McNamara, D. H., & Larsson, H. J. 1962, ApJ, 135, 748
Meyer, J. P. 1985, ApJS, 27, 21
Miller, G. E., & Scalo, J. M. 1979, ApJS, 41, 513
Moon, T. T. 1985, Comm. Univ. London Obs. 78
Moon, T. T., & Dworetsky, M. M. 1985, MNRAS, 217, 305 (MD)
Napiwotzki, R., Schönberner, D., & Wenske, V. 1992, in Lecture Notes in Physics 401, Atmospheres of Early-Type Stars, ed. U. Heber & C. S. Jeffery (Berlin, Heidelberg, New York: Springer-Verlag), 18
———. 1993, A&A, 268, 653 (NSW)
Nissen, P. E. 1988, A&A, 199, 146
Olive, K. A., & Schramm, D. N. 1982, ApJ, 257, 276
Osterbrock, D. E., Tran, H. D., & Veilleux, S. 1992, ApJ, 389, 305
Peimbert, M., Storey, P. J., & Torres-Peimbert, S. 1993, ApJ, 414, 626
Reeves, H. 1972, A&A, 19, 215
———. 1978, in Protostars and Planets, ed. T. Gehrels (Tucson: Univ. Arizona Press), 399
Rubin, R. H., Dufour, R. J., & Walter, D. K. 1993, ApJ, 413, 242
Rubin, R. H., Simpson, J. P., Haas, M. R., & Erickson, E. F. 1991, ApJ, 374, 564
Seaton, M. J., Yu, Y., Mihalas, D., & Pradhan, A. K. 1993, MNRAS, in press
Slettebak, A. E., & Howard, R. F. 1955, ApJ, 121, 102
Thielemann, F.-K., Nomoto, K., & Hashimoto, M. 1993, in Origin and Evolution of the Elements, ed. N. Prantzos, E. Vangioni-Flam, & M. Cassé (Cambridge: Cambridge Univ. Press), 297
Walter, D. K., Dufour, R. J., & Hester, J. J. 1992, ApJ, 397, 196
Warren, W. H. 1976, MNRAS, 174, 111
Warren, W. H., & Hesser, J. 1978, ApJS, 36, 497
Woosley, S. E., & Weaver, T. A. 1986, in IAU Colloq. 89, Radiation Hydrodynamics, ed. D. Mihalas & K. H. Winkler (Dordrecht: Reidel), 91